Institute for Space Nuclear Power Studies
Department of Chemical and Nuclear Engineering
The University of New Mexico
Albuquerque, New Mexico 87131

TRANSIENT AND LOAD FOLLOWING CHARACTERISTICS OF A FULLY INTEGRATED SINGLE-CELL THERMIONIC FUEL ELEMENT

MOHAMED EL-GENK, HUIMIN XUE AND CHRIS MURRAY

FINAL REPORT NO. UNM-ISNPS 3-1992

Subcontract No. S-247-002-001, UES Services Inc., Dayton, Ohio

Performance Period March 1, 1991 - February 28, 1992

March 1992

Institute for Space Nuclear Power Studies
Department of Chemical and Nuclear Engineering
The University of New Mexico
Albuquerque, New Mexico 87131

TRANSIENT AND LOAD FOLLOWING CHARACTERISTICS OF A FULLY INTEGRATED SINGLE-CELL THERMIONIC FUEL ELEMENT

MOHAMED EL-GENK, HUIMIN XUE AND CHRIS MURRAY

FINAL REPORT NO. UNM-ISNPS 3-1992

Subcontract No. S-247-002-001, UES Services Inc., Dayton, Ohio
Performance Period March 1, 1991 - February 28, 1992

March 1992

Accession Number: 4461

Publication Date: Mar 01, 1991

Title: Transient and Load Following Characteristics of A Fully Integrated Single-Cell Thermionic Fuel Element

Personal Author: El-Genk, M.; Xue, H.; Murray, C.

Corporate Author Or Publisher: Institute for Space Nuclear Power Studies, U. of NM, Albuquerque, NM 8
Report Number: UNM-ISNPS 3-1992

Descriptors, Keywords: Sincle-Cell Thermionic Fuel Element TITAM Emission

Pages: 00100

Cataloged Date: Apr 21, 1993

Contract Number: S-247-002-001,

Document Type: HC

Number of Copies In Library: 000001

Record ID: 26717

TABLE OF CONTENTS

Page

ABSTRACT iii

LIST OF FIGURES iv

LIST OF TABLES vi

NOMENCLATURE vii

1. INTRODUCTION 1

2. MODEL DESCRIPTION 2
- 2.1 Input and Output Parameters 3
- 2.2 Capabilities of TITAM 3
- 2.3 Six Groups Point-Kinetics Model 6
- 2.4 Thermal Model of the TFE 7
- 2.5 Coolant Channel Thermal-Hydraulics Model 9
- 2.6 Thermionic Emission Model 10

3. THERMIONIC EMISSION MODEL 12
- 3.1 Ignited Mode of Operation 12
- 3.2 Unignited Mode of Operation 14
- 3.3 Electrodes Work Functions Correlations 16

4. RESULTS AND DISCUSSIONS 17
- 4.1 Steady-state Operation 17
- 4.2 Effect of Coolant Temperature 22
- 4.3 Transient Operation 26
- 4.4 Load-Following Characteristics 35

5. SUMMARY AND CONCLUSION 38

ACKNOWLEDGMENT 44

REFERENCES 45

TRANSIENT AND LOAD-FOLLOWING CHARACTERISTICS OF A FULLY INTEGRATED SINGLE-CELL THERMIONIC FUEL ELEMENT

ABSTRACT

Practical application of thermionic space nuclear power systems necessitates the investigation of such systems responses to changes in operation and design parameters as well as load-following characteristics. The principle building block in these systems is the thermionic fuel element (TFE). A Thermionic Transient Analysis Model (TITAM) is developed to simulates transient and steady-state operations of a fully integrated, single-cell TFE. TITAM is used to investigate the responses of the TFE to a step input in reactivity, a change in Cs pressure and/or in the size of the interelectrode gap, a change in the coolant temperature, and a change in load demand. The effects of these parameters on load electric power, emitter temperature, overall conversion efficiency, and load-following characteristics of the TFE are determined. Results show that although nuclear reactors having negative temperature reactivity coefficients are always load-following, TFEs are only partially load-following. However, for a given load electric power need there are several combinations of fission powers and load resistances. Results also show that for TFEs having a large interelectrode gap, it is desirable to conserve Cs by lowering its vapor pressure at the beginning-of-life, since increasing the Cs pressure insignificantly affects the load electric power. However, should fuel swelling, after operating the reactor for an extended period of time, reduces the width of the interelectrode gap, both the conversion efficiency and the load electric power will decrease. In this case, the load electric power could be restored by increasing the fission power, and only partially by changing the coolant temperature and/or increasing the Cs vapor pressure.

LIST OF FIGURES

Page

Figure 1. A Schematic of the Single-cell Thermionic Fuel Element 4

Figure 2. A Line Diagram of the Building Blocks in TITAM. 5

Figure 3. Work Functions Correlations for Tungsten and Molybdenum Electrodes Based on the Data of Houston 15. 18

Figure 4. Steady-state Results Showing the Effect of Changing the Cs Pressure and the Gap Size 20

Figure 5. Steady-state Results Showing the Effect of Changing the Cs Pressure and the Gap Size on the Fuel and Emitter Temperature 23

Figure 6. Steady-state Results Showing the Effect of Changing the Cs Pressure and Gap Size on the Collector Temperature 24

Figure 7. Steady-state Results Showing the Effect of Changing the Coolant Temperature on the TFE Performance 25

Figure 8(a). Total Reactivity Transient Response to a Positive Step Input in Reactivity of $ 0.5 27

Figure 8(b). Transient Response of Fission Power and TFE Temperatures to a Positive Step Input in Reactivity of $ 0.5 28

Figure 9(a). Total Reactivity Transient Response to a Negative Step Input in Reactivity of $ 0.5 29

Figure 9(b). Transient Response of Fission Power and TFE Temperatures to a Negative Step Input in Reactivity of $ 0.5 30

Figure 10(a). Comparison of the Transient Response of Load Electrical Power to a Positive and Negative Step Input in Reactivity of $ 0.5 32

Figure 10(b). Comparison of the Transient Response of TI and TFE Conversion Efficiencies to a Positive and Negative Step Input in Reactivity of $ 0.5 .. 33

Figure 11. J-V Characteristics Illustrating the Operation Modes of the TFE Following a Positive and Negative Step Input in Reactivity of $ 0.5 34

Figure 12. Load-following Characteristics of the TFE Showing the Effect of Changing the Load Demand on Both the Load Electric Power and Fission Power 36

Figure 13. Load-following Operating Surface for the Fully Integrated, Single-cell TFE 37

Figure 14. Response of the Load Electric Power and TFE Conversion Efficiency to Changes in the Load Demand 39

Page

Figure 15. Effect of Cs Pressure and Gap Size on the J-V Characteristics and Operation of the TFE. 40

Figure 16(a). Effect of Cs Pressure and Gap Size on the Emitter Temperature and Fission Power as Functions of Load Demand. 41

Figure 16(b). Effect of Cs Pressure and Gap Size on the Load Voltage and Current as Functions of Load Demand..... 42

LIST OF TABLES

Page

Table 1. Base Case Design and Operation Parameters of the TFE 19

NOMENCLATURE

English

A	:	logarithmic mean area, cross section area flow area (cm^2), Coefficient [Eq.(32) and Eq. 18(a)]
B	:	Coefficient [Eq. 18b]
C	:	Specific heat (J/g·K)
$C_i^*(t)$	:	Equivalent concentration of delayed neutron precursors of the ith group
D_e	:	Equivalent hydraulic diameter (cm)
h	:	Heat transfer coefficient, gap conductance (W/cm^2 K), heat of adsorption of Cs (eV)
I	:	Electric current (A)
J	:	Electric current density (A/cm^2)
J_s	:	Saturation emitter electron current density (A/cm^2)
J'	:	Current density at the transition point for the ignited mode (A/cm^2)
J^*	:	Current density at the transition point for the unignited mode (A/cm^2)
Ji	:	Ion current Density (A/cm^2) [Eq. (33)]
Jn	:	Electron emission current density (A/cm^2) [Eq.(32)]
k	:	Thermal conductivity (W/cm K)
k_B	:	Boltzmann's constant (1.38054×10^{-23} J/K)
L	:	Lead length (cm)
M	:	Mass (g)
$\dot{m}$	:	Coolant mass flow rate (g/s)
P	:	Fission power, thermal power, or electric power (W), pressure (Torr)
Pe	:	Peclet number ($\dot{m}D_eC_{co}/A_{co}k_{co}$)
r	:	Radius (cm)
R	:	Electric resistance (mΩ)
T	:	Temperature (K)
T_{ee}	:	Emitter electron temperature (K)
t	:	Time (s)
V_d	:	Arc voltage drop (V)
V_{dle}	:	Voltage drop in the leads (V)
V_d'	:	Arc voltage drop at the transition point in the ignited mode (V)
V_{out}	:	Output voltage for TI converter (V)
V_{out}'	:	Output voltage at the transition point in the ignited mode (V)
Ve	:	Emitter sheath voltage drop (V)
V_{out}''	:	Output voltage at the transition point in the unignited mode (V))

Greek

Λ	:	Prompt neutron lifetime (s)
α	:	Reactivity feedback coefficients, ion current ratio
$\bar{\beta}_i$	:	:Delayed neutron fraction of the ith group
$\bar{\beta}$	:	Average delayed neutron fraction
γ	:	Annuls ratio of coolant channel (r_{co}/r_{cl})
δ	:	Interelectrode gap width (cm)
ΔV	:	Emitter space-charge voltage drop (V)
ε	:	Surface emissivity
ϕ	:	Electrode work function (eV)
λ_i	:	Decay constant of the delayed neutron precursor of the ith group (s^{-1}) [Eq.(1) and (2)]
λ	:	Effective electron mean free path (cm) [Eq. (28), (35-37)]
ρ	:	Reactivity, density (g/cm^3)
μ	:	Ion arrival rate (ion/cm^2 s) [Eq. (34)]
σ	:	Stefan-Boltzmann constant (5.669×10^{-8} W/cm^2K^4)

Subscript

c	:	Collector
Cs	:	Cesium
cl	:	Cladding
cle	:	conduction in electric leads
co	:	Coolant
e	:	Emitter, electric, electron charge
ec	:	Electric cooling
ex	:	External
f	:	Fuel
g	:	Interelectrode gap
ga	:	Fuel-emitter gap
i	:	Various regions e.g. fuel, cladding, etc. (Eq. 3-5)/ Ion current (Eq. 33)
in	:	Input, inlet
ins	:	Insulation
jle	:	Joule heating in electric leads
le	:	Electric leads
load	:	Electric load
m	:	Mean
n	:	Neutral
out	:	Output
R	:	Cesium reservoir

Superscript

c	:	Exponent (Eq. 17)
D	:	Doppler effect
E	:	Temperature effect
-	:	Average

1. INTRODUCTION

Several space exploration missions are being considered early next century which would require electric power levels ranging from tens to hundred of kilowatts. Examples of such missions include establishing an outpost on the moon and mining of its resources,[1-3] powering a manned rovers for global exploration of the Lunar and Martian surfaces,[4,5] and powering a manned rocket to Mars.[6-8] The power needed for these and other defense and civilian missions operating in high earth orbit for 3-10 years are best met with the use of nuclear reactor space power systems. Design requirements of such systems include safety during all phases of the mission (launch, deployment and end-of-life disposal), low specific mass, no single point failure, survivability, low heat rejection radiator area, and high reliability.

Nuclear reactor power systems are currently being developed under two joint DOE/DOD/NASA programs to advance the Thermionic (TI) and Thermoelectric (TE) power systems technologies[9,10] to support a potential nuclear flight demonstration program decision in mid 1990s. Both systems offer many attributes for meeting electric power needs from a few tens to hundreds of kilowatts. The TI nuclear reactor power systems have a moderately high conversion efficiency (8%-10%) and operate at higher radiator temperature (>900 K) than TE systems. The high efficiency lowers the reactor thermal power, resulting in lower masses for the reactor and shield and smaller radiator area. Also, the high radiator temperature reduces its size, resulting in smaller system's overall volume and specific mass. Like its sister TE systems, TI systems promote high reliability, due to the lack of moving parts, and redundancy, since a failure of a single converter unit will have little effect on the performance of other unites in the system. However, since TI converters could be used both in-core or ex-core, they provide the system designer a flexibility in integrating the system components for enhanced overall reliability at a potential reduction in the overall system mass and volume.

An important issue related to the development of TI space nuclear power systems is understanding the effects of various operation and design parameters on the steady-state and transient performance of the fully integrated power system, or the thermionic fuel elements (TFEs),

which are the basic building blocks. Some of these parameters include changes in reactor thermal power due to a reactivity insertion, changes in the width of interelectrode gap due to fuel swelling, changes in Cesium (Cs) vapor pressure in the interelectrode gap, and changes in the load demand. In order to quantify the effects of these parameters, an integrated system or TFE model needs to be developed, which directly couples the TI converter units to both the electric load and the nuclear fuel region and incorporates nuclear reactor kinetics with the appropriate reactivity feedbacks.

Existing models are limited to the analysis of steady-state operation of either a TI diode[11] or a TFE.[12,13] The input to the TI diode model includes the emitter and collector temperatures and the emission current density. The TFE model of Pawlowski et al.[12] basically couples the TI diode model to a two-dimentional, steady-state thermal-hydraulic model. Because this model is not directly coupled to the electric load and reactor kinetics, the load current and fission power must be specified in the input. In addition, both models[11,12] do not include the unignited mode of TI emission, hence, are not suited for startup simulation.

The objective of the research is to develop a transient model of a fully integrated single-cell TFE, which directly couples the electric load to the TI converter and incorporates neutron kinetics with the appropriate reactivity feedback effects. The model is used to investigate the effects of a reactivity step-function input, a change of the Cs vapor pressure and/or the width of the interelectrode gap, and a change in the coolant temperature on the TI conversion efficiency, load electric power and TI converter temperatures. The load-following characteristics are also investigated and the operation regimes in which the TFE is inherently load-following are identified as functions of fission power and load demand.

2. MODEL DESCRIPTION

The Thermionic Transient Analysis Model (TITAM) is developed to simulate transient and steady-state operations of a fully integrated TFE with either fission heating or electric heating. The fission heating option could be used to predict the performance characteristics of in-core TFEs, while the electric heating option would be useful in comparing the model predictions with test

results of electrically heated TFEs. TITAM consists of four interactively coupled sub-models: (1) a nuclear reactor six groups point-kinetics model, (2) a lumped transient thermal model of the integrated nuclear fuel element and TI converter, (3) a thermal-hydraulics model of the liquid metal coolant channel, and (4) a thermionic emission model.[14] The work functions of the emitter and the collector materials in the TI emission sub-model are determined as functions of the electrode-Cs reservoir temperature ratio using correlations based on the low Cs pressure data of Houston.[15] Ongoing effort is directed toward updating these correlations based on high pressure data (up to 20 torr) and/or phenomenological modeling.[14]

2.1 Input and Output Parameters

In the fission heating option, the input to TITAM includes the dimensions and materials of the TFE, temperature reactivity feedback coefficients of the different regions of the TFE, cesium reservoir temperature, load electric resistance, either fission power or reactivity input to the reactor core, and the coolant inlet temperature and mass flow rate. The output parameters includes electric power to the load, load current and voltage, conversion efficiency, and temperatures in the different regions of the TFE. For electrically heated TFE, the input and output parameters are the same as for the fission heating option, except that fission power/reactivity input is replaced by electric power input, with no reactivity feedback effects. As a user option the dimensions of the electric leads could be optimized for minimum electric and thermal losses. Figure 1 presents a schematic and the electric circuit of the single-cell TFE model and Fig. 2 presents a line diagram of the building blocks in TITAM.

2.2 Capabilities of TITAM

In addition to transient and steady-state simulation, TITAM could be used for design and operation optimization of single cell TFEs and/or of a TI power system. An example of potential in-core application of TITAM is mapping the design parameters in the nuclear reactor core for maintaining a constant emitter temperature and assessing the effects of non-uniform radial and axial

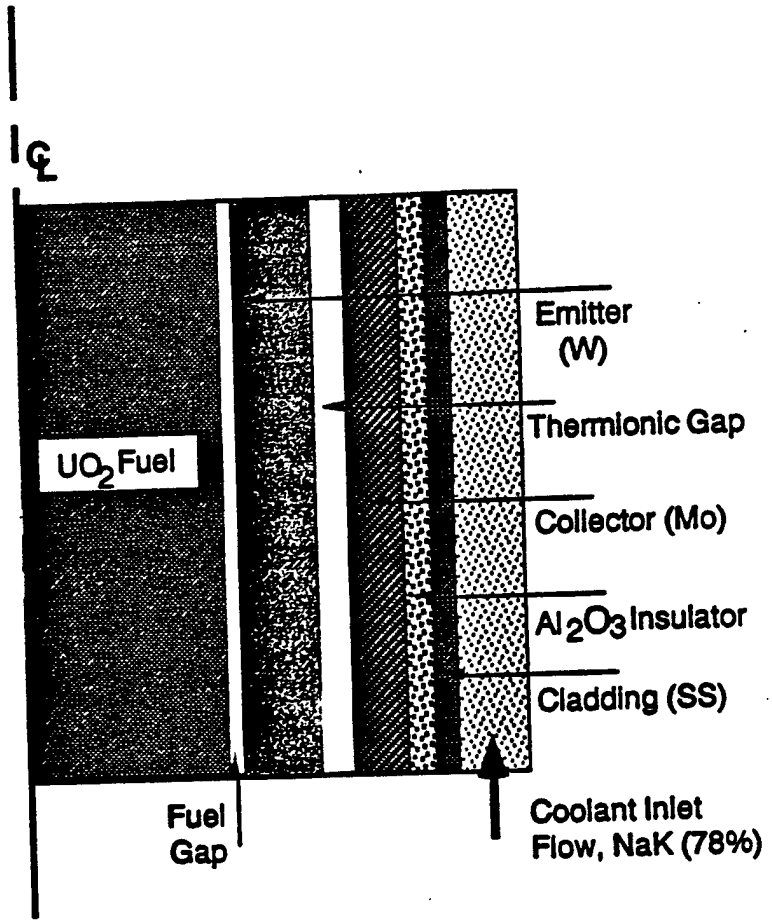

Figure 1. A Schematic of the Single-cell Thermionic Fuel Element

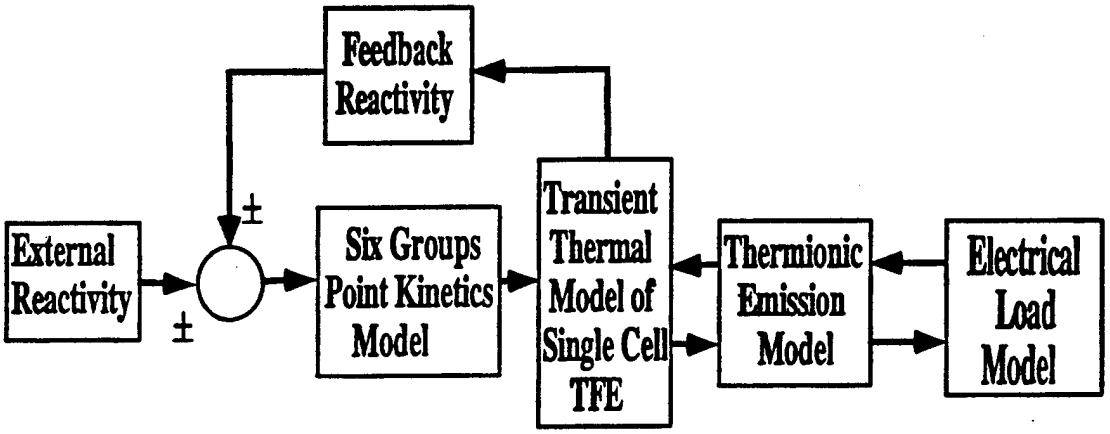

Figure 2. A Line Diagram of the Building Blocks in TITAM.

distributions of fission power in the reactor core on the performance of the TFEs. Examples of other applications include: (a) determining the operation regime where the TFEs or the TI power system is inherently load-following, (b) determining the effect of using high temperature heat pipe to equalize the temperature along the emitter on the TFE performance, (c) developing an operation strategy for optimizing the consumption of Cs over the lifetime of the system, and (d) determining the effects of using a low pressure Cs-Ba vapor mixture (< 0.1 torr), instead of the high pressure Cs vapor (2-10 torr), on the performance of a new generation of high performance TFEs.

The TI sub-model in TITAM incorporates both the ignited and the unignited modes of emission, which makes it suitable for both high temperature and low temperature simulations including startup and shutdown transients. Because the work functions of the electrode are determined in terms of the Cs reservoir temperature and those of the electrodes, TITAM could be used to investigate the effects of changing the Cs pressure on the load electric power, overall conversion efficiency, and the load-following characteristics of the TFE. As indicated earlier, in addition to simulating the operation of a fission-heated single cell TFE, by including temperature and Doppler reactivity feedback effects, TITAM is capable of simulating electrically heated TFEs which could be tested in a laboratory setup. Therefore, the user would be able to relate the performance of electrically-heated TFEs to that of fission heated TFEs, without the expense and complication of fission-heated tests. The component models shown in Fig. 2 are discussed in detail in the following sections.

2.3 Six Groups Point-Kinetics Model

The six groups point-kinetics model in TITAM calculates the transient fission thermal power following an external reactivity insertion and incorporates reactivity feedback due to Doppler and temperature effects. The nuclear reactor point-kinetics equations may be expressed as :

$$\frac{dP_{in}(t)}{dt} = \frac{\rho(t) - \bar{\beta}}{\Lambda} P_{in}(t) + \sum_{i=1}^{6} \lambda_i C_i^*(t) \quad \text{,and,} \qquad (1)$$

$$\frac{dC_i^*(t)}{dt} = \frac{\beta_i P_{in}(t)}{\Lambda} - \lambda_i C_i^*(t) \qquad (i=1,2,..,6) \tag{2}$$

The total reactivity input to the reactor core is given as:

$$\rho(t) = \rho_{ex}(t) + \rho_f^D(t) + \sum_i \rho_i^E(t) \tag{3}$$

The first term on the R.H.S of Eq. (3) is the external reactivity input to the nuclear reactor core. The second and third terms in Eq. (3) are the reactivity feedback due to Doppler effect in the fuel region, $\rho_f^D(t)$, and $\rho_i^E(t)$ is the sum of temperature reactivity feedback effects in different regions of the TFE. The Doppler feedback reactivity and the temperature feedback reactivity in any given region, i, in the TFE [see Fig. 1] are expressed, respectively, as:

$$\rho_f^D(t) = \alpha_f^D \ln\left(\overline{T_f}(t)/\overline{T_f}(0)\right) \tag{4}$$

and,

$$\rho_i^E(t) = \alpha_i^E\left(\overline{T_i}(t) - \overline{T_i}(0)\right) \tag{5}$$

2.4 Thermal Model of the TFE

The thermal sub-model in TITAM calculates the average transient and steady-state temperatures in the various regions of the TFE [see Fig. 1] including the emitter, collector, insulation, cladding, and liquid-metal coolant in the cooling channel, as functions of fission power (or reactivity input), coolant flow rate and inlet temperature, width of interelectrode spacing, Cs vapor pressure, and other design parameters. The average fuel and fuel/emitter gap temperatures during a transient are given, respectively, as:

$$M_f C_f \frac{dT_f}{dt} = P_{in} - h_f A_f (T_f - T_{ga}) \tag{6}$$

$$M_{ga} C_{ga} \frac{dT_{ga}}{dt} = h_f A_f (T_f - T_{ga}) - h_{ga} A_{ga} (T_{ga} - T_e), \tag{7}$$

where $h_f = (2\ k_f/r_f)$. For an open fuel/emitter gap the gap conductance is calculated as:

$$h_{ga} = \left(\frac{k_{ga}}{\delta_{ga}}\right) + \left(\frac{3\ \sigma T_{ga}^3}{1/\varepsilon_f + 1/\varepsilon_e - 1}\right), \tag{8}$$

where $\varepsilon_e = f(\overline{T}_{fe})$ and $\overline{T}_{fe} = \sqrt{T_f T_e}$. The average emitter temperature and that of the interelectrode gap are given, respectively, as:

$$M_e C_e \frac{dT_e}{dt} = h_{ga} A_{ga} (T_{ga} - T_e) - h_e A_e (T_{ga} - T_e) - h_{le} A_{le} (T_e - T_c) - P_{ec} + \frac{1}{2} P_{jle} \tag{9}$$

$$M_g C_g \frac{dT_g}{dt} = h_e A_e (T_e - T_g) - h_g A_g (T_g - T_c) \tag{10}$$

In Eq. (10), the radiation and conduction contributions to heat transfer between the emitter and the collector are incorporated in the gap conductance, h_g, as:

$$h_g = \left(\frac{k_g}{\delta_g}\right) + \left(\frac{3\ \sigma T_g^3}{1/\varepsilon_e + 1/\varepsilon_c - 1}\right) \tag{11}$$

In this equation, $\varepsilon_e = f\ (T_e)$, but $\varepsilon_C = f\ (\overline{T}_{ec})$, where $\overline{T}_{ec} = \sqrt{T_e T_c}$. The thermal conductivity of Cs vapor in the interelectrode gap, k_g, is determined in terms of its vapor pressure as:[16]

$$k_g = \frac{1.65\ x\ 10^{-6}\ \sqrt{T_m}}{\delta_g + 1.14\ x\ 10^{-5} \left(\frac{T_e + T_c}{P_{Cs}}\right)}, \tag{12a}$$

where,

$$T_m = (4/9)\left(\frac{T_e^{1.5} - T_c^{1.5}}{T_e - T_c}\right)^2 \qquad (12b)$$

The transient temperatures of the collector, insulator and cladding are given, respectively, as:

$$M_c C_c \frac{dT_c}{dt} = h_g A_g (T_g - T_c) - h_c A_c (T_c - T_{ins}) + h_{le} A_{le} (T_e - T_c) + P_{ec} + \frac{1}{2} P_{jle} - P_e \qquad (13)$$

$$M_{ins} C_{ins} \frac{dT_{ins}}{dt} = h_c A_c (T_c - T_{ins}) - h_{ins} A_{ins} (T_{ins} - T_{cl}) \qquad (14)$$

and,

$$M_{cl} C_{cl} \frac{dT_{cl}}{dt} = h_{ins} A_{ins} (T_{ins} - T_{cl}) - h_{cl} A_{cl} (T_{cl} - T_{co}) \qquad (15)$$

2.5 Coolant Channel Thermal-Hydraulics Model

The transient bulk temperature of the liquid-metal coolant in the annular flow channel of the TFE [see Fig. 1] is determined from the relation:

$$M_{co} C_{co} \frac{dT_{co}}{dt} = h_{co} A_{co} (T_{cl} - T_{co}) - 2\dot{m} C_{co} (T_{co} - T_{in}), \qquad (16)$$

where the heat transfer coefficient for concentric annuli is given as:[17]

$$h_{co} = (k_{co}/D_e)(A + B\, Pe^q), \qquad (17)$$

where,

$$A = 4.63 + 0.686\ \gamma, \qquad (18a)$$

$$B = 0.215 + 4.3\text{x}10\text{-}5\ \gamma, \qquad (18b)$$

$$c = 0.752 + 0.01657\ \gamma - 8.83\text{x}10^{-4}\ \gamma^2. \qquad (18c)$$

During steady-state simulation the terms on the left-hand side of Eqs. (6), (7), (9), (10), (13), (14), (15) and (16) are dropped out and the temperatures in the different regions of the TFE are calculated using an iterative explicit approach. In this case, the iterations are only for the sole purpose of updating the thermophysical properties in the various regions as functions of their respective temperatures.

2.6 Thermionic Emission Model

The structure of the TI emission model in TITAM follows closely the phenomenology developed by Rasor,[14] which takes into account the continuity of electron and ion emission currents, and energy fluxes at the plasma-electrode interfaces and across the plasma. The complex collisional effects in the plasma have been neglected. The thermionic emission model calculates the electric power delivered to the load in a self-consistent manner with the thermal sub-model discussed earlier. The TI emission model include both the ignited and unignited modes of operation. Also, the transition conditions between the saturated and obstructed regimes in each mode are included in the models. The overall energy balance in the thermionic emission model includes electron cooling, heat conduction through the interelectrode gap, and heat conduction and Joule heating in the electric leads. The characteristic equations describing these processes are:

Electron Cooling

$$P_{ec} = JA_e\left(\frac{\phi_e}{e} + \frac{2k_B T_e}{e}\right) \tag{19}$$

Heat Conduction in the interelectrode gap

$$P_g = h_g A_g (T_e - T_c) \tag{20}$$

Heat Conduction through the leads

$$P_{cle} = (k_{le} / L_{le}) A_{le} (T_e - T_c) . \tag{21}$$

Joule heating in the leads

$$P_{jle} = (JA_e)^2 R_{le} . \tag{22}$$

A steady-state the overall energy balance for the TI converter yields :

$$P_{in} - P_{out} = P_{load} \text{ , where,} \tag{23}$$

$$P_{in} = P_{ec} + P_g + P_{cle} - 0.5\, P_{jle}, \tag{24a}$$

$$P_{load} = A_e J V_{load}, \tag{24b}$$

and,

$$V_{load} = V_{out} - V_{dle}, \text{ and } V_{dle} = JA_e R_{le}. \tag{25}$$

A quasi-steady state approach is used to couple Eq. (23) with the transient thermal model when simulating the transient operation of the TI converter. During each small time step in the thermal model it is assumed that the conditions governing thermionic emission are constant, but different from those in the previous and subsequent time steps. This approach should be fairly accurate when the time step is small enough, depending of the stiffness of the problem. In fact, because the stiffness of the reactor kinetics equations, the time step used for transient fission power calculations (~ 0.1 sec), easily satisfied the requirements for the quasi-steady state solution of the TI emission model. This conclusion is reached when it is found that a decrease in the time step,

beyond that dictated by the reactor kinetics equations, does not practically change the results. Also, to ensure numerical stability of the transient solution and flexibility in the selection of the time step, an implicit time-integration approach is used to solve the governing equations in the thermal model of the TFE.

3. THERMIONIC EMISSION MODEL

The emitter and collector temperatures, cesium pressure, and electrode work functions determine the operating mode of the TI converter. At lower temperatures, the converter is in the unignited mode and at higher temperatures (>1300 K) the converter is in the ignited mode. In each mode, the output voltage (V_{out}) is determined from the J-V characteristics for that mode. The TI emission models for the ignited and unignited modes of operation are presented in the following sub-sections.

3.1 Ignited Mode of Operation

In the ignited mode of operation, the inelastic collisions in the interelectrode space is the dominant ionization mechanism of Cs atoms in the gap. The current discharge in the gap is sustained by the potential drop across the interelectrode space, V_d. When Cs ions generated in the gap by inelastic collisions are just sufficient to neutralize the space charge, the converter is said to be operating at the transition point, (J', V'_{out}), when:

$$V_{out} = \phi_e - \phi_c - V'_d \tag{26}$$

The transition point thus corresponds to the minimum voltage drop required to fully neutralize the space charge for a given $P_{Cs}d$, resulting in a maximum conversion efficiency. The cesium vapor pressure in the interelectrode gap can be expressed in terms of the cesium reservoir temperature as:[18]

$$P_{Cs} = \frac{2.45x10^8}{\sqrt{T_R}} \exp\left(\frac{-8910}{T_R}\right). \quad (27)$$

In the ignited mode of operation there are two distinct regions which intersect at the transition point; the obstructed ignited emission region ($V_{out} > V'_{out}$) and the saturation ignited emission region ($V_{out} < V'_{out}$). These two regions are characterized by distinctly different processes. In the obstructed region, because V_d is insufficient to fully neutralize the space charge a negative space charge barrier DV forms at the emitter. This potential barrier reduces the electron emission current, thus making space charge neutralization possible. In the obstructed ignited region, the discharge current is given as:[14]

$$J = \frac{J_e}{1 + \left(\frac{3\delta_g}{4\lambda} + R\right). \exp\left(\frac{-V_e}{k_B T_{ee}}\right)}, \quad (28)$$

and the output voltage is given as:

$$V_{out} = \phi_e - \phi_c - V_d + \Delta V, \quad (29)$$

where J_e, R, V_e T_{ee}, $\left(\frac{\delta_g}{\lambda}\right)$, are defined by Eqs. (9), (24-29), and (31) in Ref.14.

In the saturation ignited region, V_d is greater than V'_d, which is required to completely neutralize the space charge. The excess potential, $-\Delta V = (V_d - V'_d)$ in the emitter sheath generates positive ions, which move toward the emitter giving rise to a positive ion current. The electric field created at the emitter surface lowers the emitter's effective work function, hence increasing the electron emission by Schottky effect. The output current in the saturated ignited region can be expressed as:

$$J = \frac{J_s}{1 + (\frac{J_s'}{J'} - 1) exp\,(\frac{\Delta V}{k_B T_{ee}})}, \qquad (30)$$

where J' is the current density at the transition point, J_s' and J_s are given by Eqs. (1), (2) and (35) in Ref. (14). Eqs. (27-30) are solved iteratively to determine the transition point and generate the J-V curves which are characteristic of the design, electric load, and operating conditions of the TI converter.

3.2 Unignited Mode of Operation

In the unignited mode of operation, surface ionization is the dominant mechanism for maintaining neutral plasma in the interelectrode gap of the converter. In this mode of operation, volume ionization is absent and the plasma potential can be expressed as:

$$\phi_n = 0.5 \left[h\,(T_e / T_R) + V_i - k_B T_e ln\,(\alpha_e D / 2AT_e^2) \right], \qquad (31)$$

where $h = 0.76\ eV$ and $V_i = 3.89\ eV$. The electron emission current is given as:

$$J_n = AT_e^2 exp\left(\frac{-\phi_n}{k_B T_e}\right). \qquad (32)$$

This electron current is partially neutralized by the ion current, which is given by the Saha-Langmuir equation as:[18]

$$J_i = e\,\mu \left[1 + 2\ exp\left(\frac{V_i - \phi_n}{k_B T_e}\right) \right]^{-1}. \qquad (33)$$

In this equation, the ions arrival rate, μ, is given as:

$$\mu = D\ exp\,(-h / k_B T_R) \qquad (34)$$

In Eq. (32), A = 120 A/m^2 K^2 and in Eq. (34), D is taken equal to $(10^{29}/\sqrt{T_R})$ atoms/cm^{2}sec[14]. In the unignited mode of operation, there are three regions of interest: (a) retarding region ($V_{out} > V_{out}^{"}$), (b) transition point, ($J^{"}$, $V_{out}^{"}$), and (c) plasma saturation region ($V_{out} < V_{out}^{"}$). At the transition point, ($J^{"}$, $V_{out}^{"}$), which corresponds to the condition of zero electric field at the collector (no collector sheath), the current density and voltage relations are :

$$J^{"} = J_n\left(\frac{3\delta_g}{4\lambda} + 1\right)^{-1}, \text{ and } V_{out}^{"} = \phi_n - \phi_c \tag{35}$$

In the retarding region ($V_{out} > V_{out}^{"}$) the current density is given as:

$$J = J_n\left[(3\delta_g/4\lambda) + exp\left((V_{out} - V_{out}^{"})/k_B T_e\right)\right]^{-1}. \tag{36}$$

In the plasma saturation region ($V_{out} < V_{out}^{"}$), the current density is limited by the ions reflected from the collector sheath and is given by:

$$J = 2J^{"} - J_n\left[(3\delta_g/4\lambda) + exp\left((V_{out}^{"} - V_{out})/k_B T_e\right)\right]^{-1}. \tag{37}$$

Equations (31-37) are solved iteratively to determine the J-V characteristics of the TI converter in the unignited mode for various design, electric load, and operating conditions.

At the transition between the ignited and unignited modes of operation, the proper operation regime for the TI converter is determined by the model, depending on whether the TFE is in a startup or a shutdown phase. During the startup of the TFE, the TI converter operates initially in the unignited mode, where the emission current increases and the arc voltage drop decreases as the fission input power is increased. When the voltage drop in the converter decreases below that corresponding to the intersect between the ignited and unignited characteristic curves, there are two

possible values of the emission current, the low value describes the converter operation in the unignited mode, and the higher value corresponds to the operation in the ignited mode. In this case the model takes the higher emission current and declares the TI converter operating in the ignited mode. Beyond this point, further increase in fission power results in higher emission current and lower voltage drop, however, the operation regime (saturated or obstructed) is determined by comparing the values of J and V_{out} with those corresponding to the transition point , (J', V'_{out}).[14] During shutdown, or a decrease in the fission power of the TFE, a similar, but opposite logic is used in the model to determine the transition from the ignited to the unignited mode of operation.

3.3 Electrodes Work Functions Correlations

The effective work function of the electrode depends on the degree of cesium coverage of its surface, which depends upon the electrode surface temperature and the Cs vapor pressure in the interelectrode gap. Using a semi-empirical curve-fits of low Cs pressure experimental data, [15] the work functions are correlated in terms of the ratio of the temperature of the emitter or collector to the cesium reservoir temperature as follows:

Tungsten Emitter

$$\phi_e(W) = 1.683 + 1.691(T_e/T_R) - 2.646(T_e/T_R)^2 + 1.321(T_e/T_R)^3 - 0.244(T_e/T_R)^4 + 0.0152(T_e/T_R)^5. \quad (38)$$

Molybdenum Collector

$$\phi_c(Mo) = 1.1173 + 2.0169(T_c/T_R) - 1.7643(T_c/T_R)^2 + 0.4405(T_c/T_R)^3 \text{ , for } (T_c/T_R) < 2.65, \quad (39a)$$

$$\phi_c(Mo) = -7.29 + 5.23(T_c/T_R) - 0.53(T_c/T_R)^2 + 0.07(T_c/T_R)^3 + 0.02(T_c/T_R)^4 - 7.11\times10^{-4}(T_c/T_R)^5 ,$$
$$\text{for } (T_c/T_R) \geq 2.65 \quad (39b)$$

These correlations are compared in Fig. 3 with the low pressure data of reference (15). As this figure indicates the correlations fits the data to within ± 5%.

4. RESULTS AND DISCUSSIONS

The steady-state and transient analyses presented herein are for optimized electric leads and for the TFE base case design and operation parameters listed in Table 1. The following subsections present steady-state, transient, and load-following results for a fully integrated, single-cell TFE. The steady-state results show the effects of changing the fission power, Cs pressure in the interelectrode gap, the size of the interelectrode gap, and the coolant temperature on the TFE's load electric power, temperatures, and conversion efficiency. The transient results delineate the response of the TFE to both a step-function increase and a step-function decrease in reactivity. Transient results include the fission power, load electric power, and the TFE temperatures and the overall conversion efficiency. The overall conversion efficiency of the TFE is defined herein as ***the ratio of the load electric power to the actual fission power generated in the TFE during the transient.*** At steady-state, the fission power is equal to the thermal power supplied to the emitter. However, during a transient increase or decrease in fission power, the corresponding thermal power to the emitter is, respectively, lower or higher than the fission power. Consequently, the TFE conversion efficiency during a transient would be markedly different than the TI converter efficiency. The load-following results define the operation regimes and the ranges of operating parameters for which the TFE is inherently load-following and those causing the TFE to be nonload-following.

4.1 Steady-State Operation

Figure 4 presents the effects of fission power, Cs pressure, and size of the interelectrode gap on steady-state electric power to the load and the TFE conversion efficiency. Results show that for the smaller gap size (0.094 mm) increasing the Cs pressure generally results in both higher electric power to the load and higher conversion efficiency, however, the effect is more pronounced at

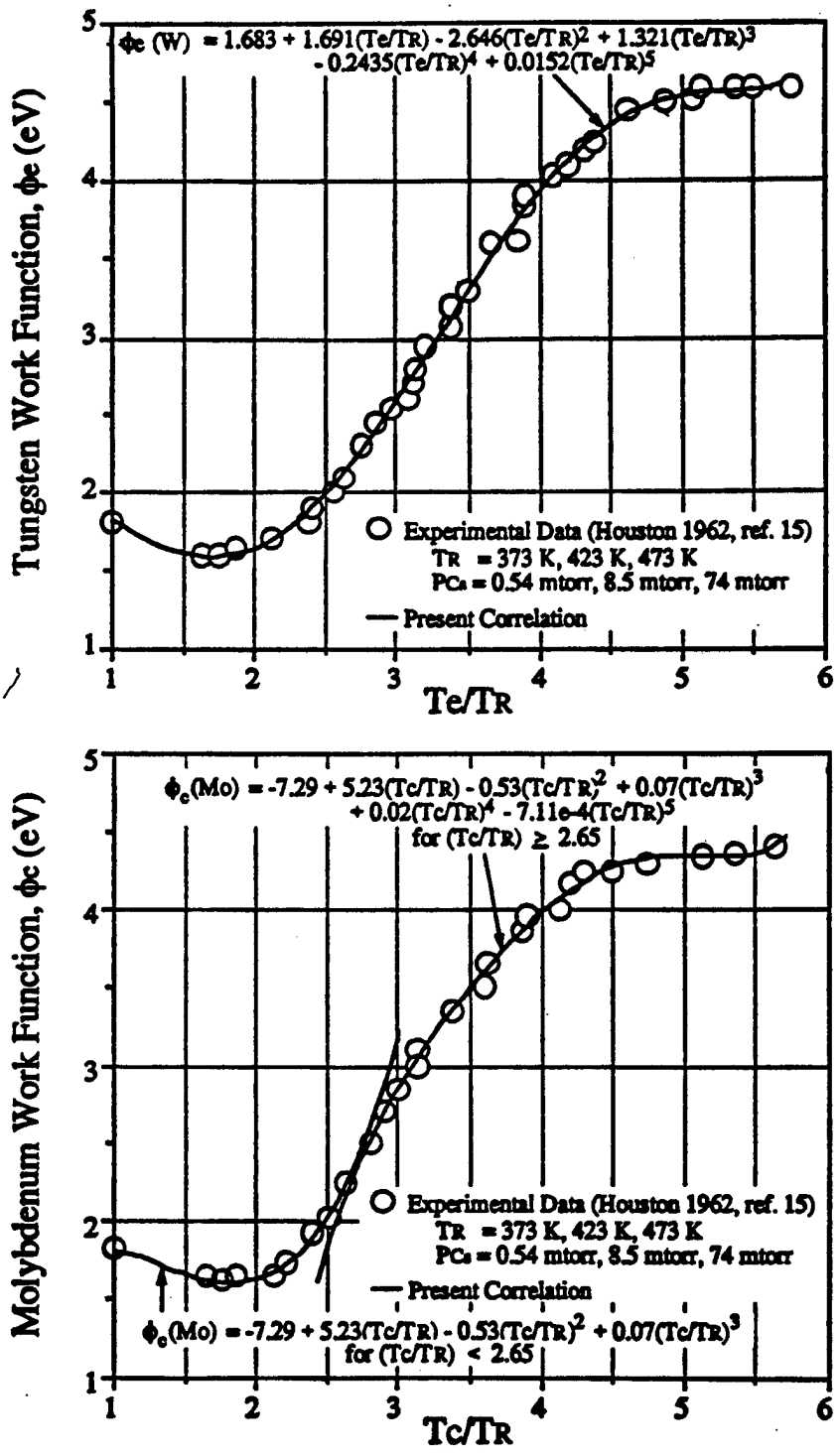

Figure 3. Work Functions Correlations for Tungsten and Molybdenum Electrodes Based on the Data of Houston [15].

Table 1. Base Case Design and Operation Parameters of the TFE

Parameter	Value
DIMENSIONS	
TI Cell Height (cm)	8.532
Fuel Gap Size (mm)	0.01
Interelectrode Gap width (mm)	0.25
Emitter Thickness (cm)	0.192
Collector Thickness (cm)	0.15
Insulation Thickness (cm	0.1
Cladding Thickness (cm)	0.15
Coolant Channel Width (cm)	1.0
Radius of Fuel region (cm)	1.205
MATERIALS	
Emitter Material	W
Collector Material	Mo
Insulation Material	Al_2O_3
Cladding Material	Stainless- Steel
Coolant	NaK(78%)
Fuel material	UO_2
OPERATING CONDITIONS	
Coolant Inlet Temperature (K)	850
Coolant Mass Flow Rate (g/s)	55.0
Load Resistance (mΩ)	
For Steady-State Analysis	5.0
For Transient Analysis	2.5
Initial Steady-State Fission Power (W)	1000
Nominal Cs Reservoir Temperature (K)	567
REACTIVITY FEEDBACK COEFFICIENTS	
Fuel Temperature Reactivity Feedback Coefficient	-1.2×10^{-5}
Emitter & Collector Temperature Reactivity Feedback Coefficient	-6.1×10^{-6}
Insulator Temperature Reactivity Feedback Coefficient	-8.7×10^{-6}
Cladding Temperature Reactivity Feedback Coefficient	-1.0×10^{-5}
Coolant Temperature Reactivity Feedback Coefficient	-2.0×10^{-6}
Fuel Doppler Reactivity Feedback Coefficient	-0.8×10^{-6}

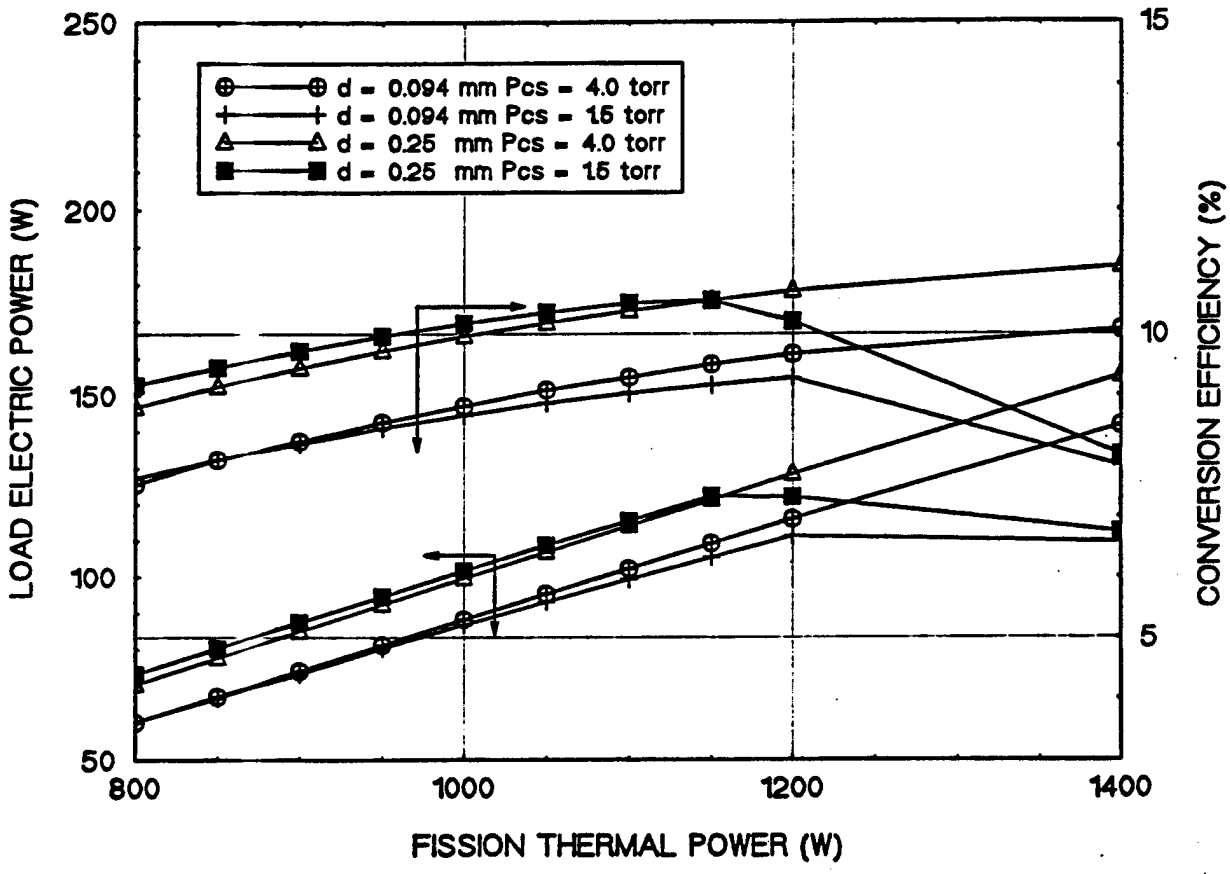

Figure 4. Steady-state Results Showing the Effect of Changing the Css Pressure and the Gap Size on the TFE Performance.

fission powers larger than 1150 W. These results are also true for the larger gap size (0.25 mm) at fission powers in excess of 1150 W. At lower fission powers, however, increasing the Cs pressure in the larger gap results in slightly lower conversion efficiency and lower electric power to the load.

Results in Fig. 4 show that the performance parameters of the TFE at a low and high Cs pressures are almost identical at fission powers below 1150 W, but are significantly different at higher fission powers. At a low fission power (< 1150 W), increasing the Cs pressure negligibly affects the operation of the TFE, while increasing the gap size always results in both higher electric power to the load and higher conversion efficiency. For example, at a Cs pressure of 4 torr the load electric power increases monotonically with fission power, and increasing the gap size from 0.094 mm to 0.25 mm increases the electric power to the load by about 15% and 50% at a fission power of 1400 W and 800 W, respectively. Conversely, at the low Cs pressure (1.5 torr), both the load electric power and conversion efficiency increase with fission power until they reach maximum values, then they decrease as the fission power is increased. Note that decreasing the gap size decreases the maximum conversion efficiency and the maximum load electric power, but increases the corresponding fission powers. For example, at a Cs pressure of 1.5 torr and gap size of 0.25mm, both the maximum efficiency (~ 10.8%) and the maximum electric load (~ 122 W) occur at a fission power of 1150 W. However, when the gap size is reduced to 0.094 mm, the maximum conversion efficiency and load electric power decrease to 9.2% and 106 W, respectively, but the corresponding fission power increases to 1200 W.

In summary , the results in Fig. 4 suggest that increasing the gap size always enhances the performance of the TFE, while increasing the Cs pressure in the interelectrode gap insignificantly affects the TFE performance at low fission powers, but markedly enhance its performance at high fission powers. However, for TFE load-following consideration it is desirable to operate at fissions powers below that corresponding to the maximum load electric power. As such fission powers, it is advisable to lower the Cs pressure, hence reducing its consumption, with little effect on the TFE performance. On the other hand, the results clearly demonstrate that a reduction in the

gap size due to swelling of nuclear fuel would strongly degrade the performance of the TFE.

Figures 5 and 6 present the results on the effect of fission thermal power on the the steady-state temperatures of the UO_2 fuel, W-emitter, and the Mo-collector. These Figures indicate the steep rise in both the fuel and emitter temperatures as the fission power of the TFE is increased. For example, increasing the fission power from 800 W to 1400 W, causes the fuel and emitter temperature to increase from approximately 2200 k to 3050 K, and from 1700 K to 1920 K, respectively. Also, the corresponding collector temperature increases from 945 K to 1020 K [see Fig. 6]. Results in Figs. 5 and 6 show that increasing either the gap size or the Cs pressure insignificantly affects the temperatures of the TFE.

4.2 Effect of Coolant Temperature

The results on the effect of the coolant inlet temperature on the TFE conversion efficiency and the load electric power are shown in Fig. 7. As this figure demonstrates, the inlet temperature of the NaK coolant strongly affects both the overall efficiency of the TFE and the electric power to the load, particularly at high fission power. For a gap size of 0.25 mm, Cs pressure of 1.5 torr, and fission powers in excess of 1100 W, decreasing the coolant inlet temperature causes both the conversion efficiency and load electric power to increase. Conversely, at lower fission powers, decreasing the inlet coolant temperature causes both the conversion efficiency and load electric power to decrease.

It is worth noting that the fission power corresponding to the maximum load electric power (~ 1200 W) is independent of the coolant inlet temperature, while that corresponding to the maximum conversion efficiency increases as the coolant inlet temperature is decreased. Figure 7 shows that at a fission power of 1400 W, lowering the coolant inlet temperature to the TFE from 850 K to 800 K, causes both the TFE conversion efficiency and the electric power to the load to increase by about 12%, from ~ 8% to 9% and from 112.5 W to 126 W, respectively. However, in the load-following region, at a fission power of 800 W, lowering the inlet coolant temperature

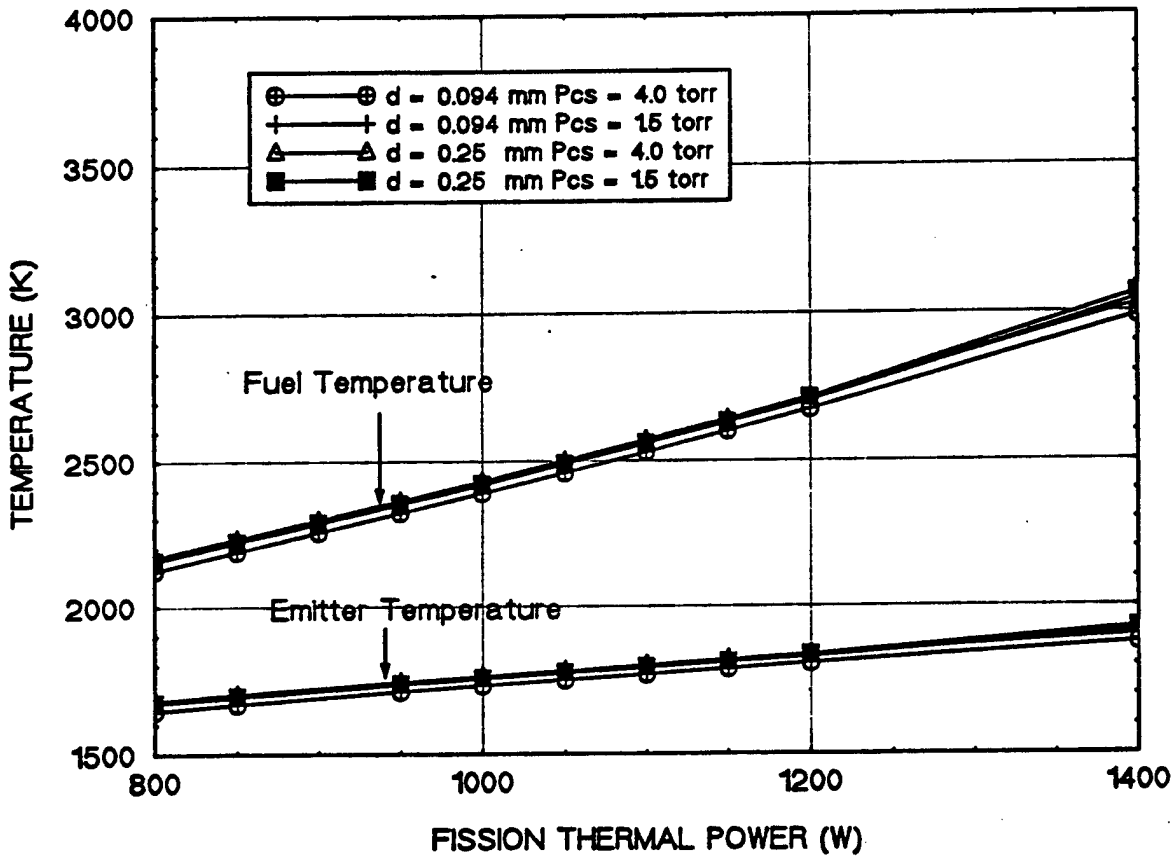

Figure 5. Steady-state Results Showing the Effect of Changing the Cs Pressure and the Gap Size on the Fuel and Emitter Temperature.

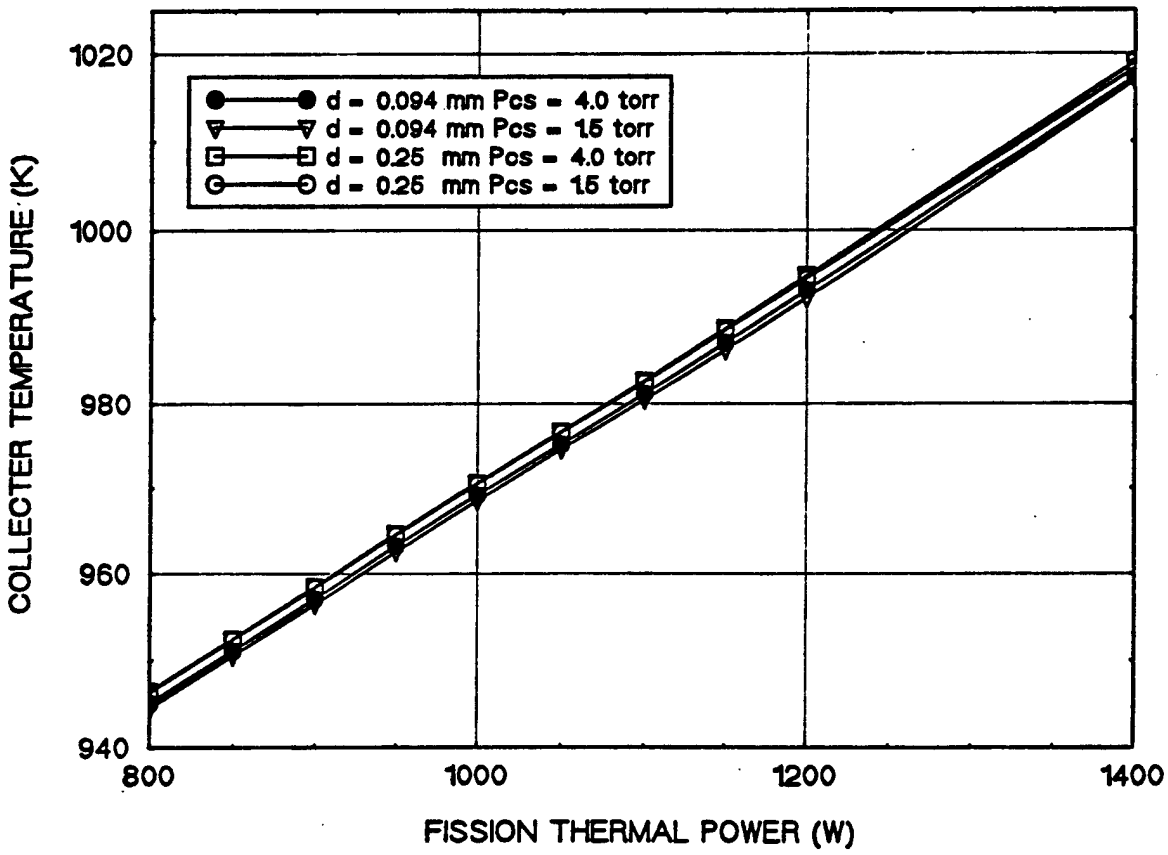

Figure 6. Steady-state Results Showing the Effect of Changing the Cs Pressure and Gap Size on the Collector Temperature.

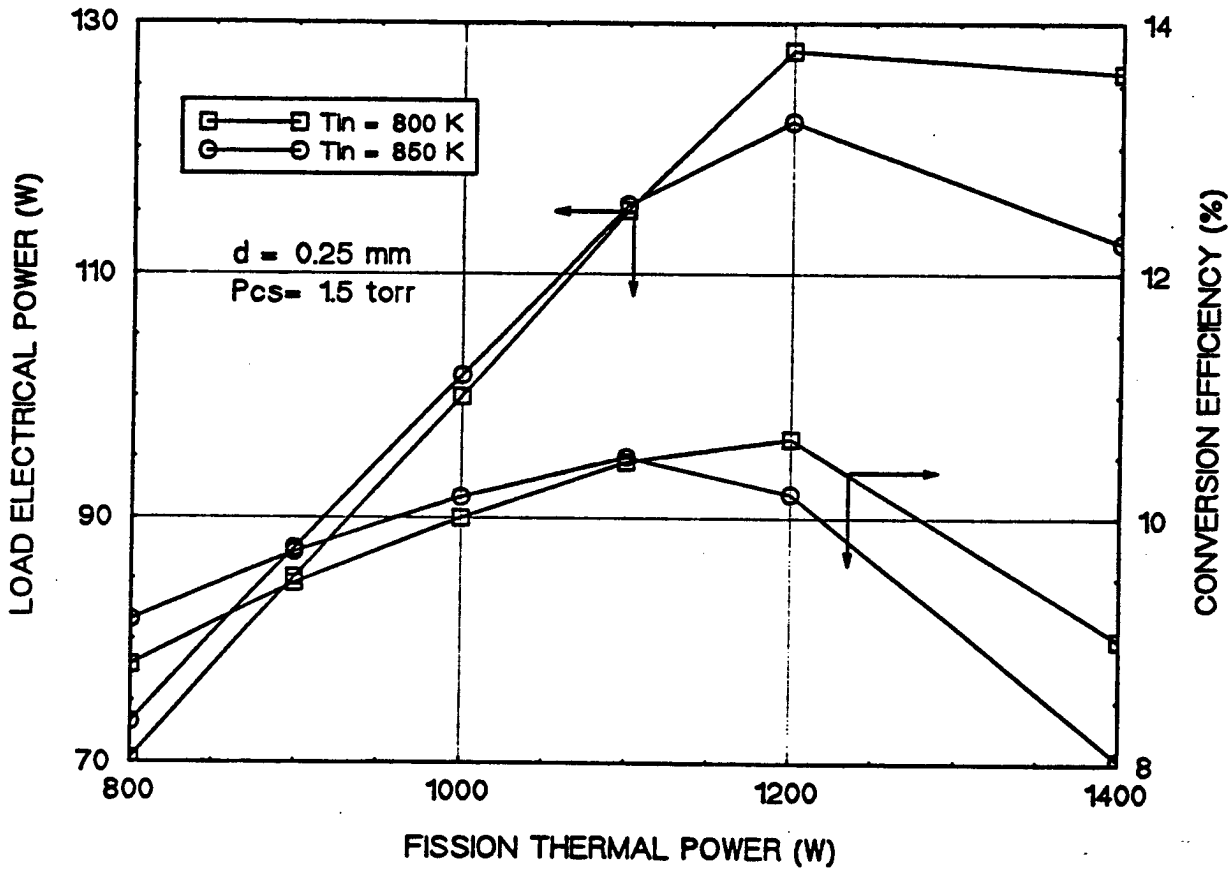

Figure 7. Steady-state Results Showing the Effect of Changing the Coolant Temperature on the TFE Performance

from 850 K to 800 K, causes both the TFE conversion efficiency and the electric power to the load to decrease by about 4.5 %, from ~ 9.2 % to 8.8% and from 73 W to 70 W, respectively.

In summary, the coolant inlet temperature could be used, in addition to the Cs pressure, to regulate the operation of the TFEs. When operating at high fission power, where the TFE is non-load following, lowering the inlet coolant temperature and/or increasing the Cs pressure would improve the TFE performance. Conversely, when operating at low fission power, where the TFE is load-following, the coolant inlet temperature may be increased to improve the performance of the TFE.

4.3 Transient Operation

Figures 8(a) and 8(b) present the changes in the total reactivity, fission power, and temperatures of the fuel, emitter and collector, following a \$0.5 positive step input in reactivity. In these Figures the initial steady-state fission thermal power before the transient is 1,000 W [see Fig. 8(b)]. Figure 8(b) shows the fission power and the temperatures of the TEF increasing initially very rapidly due to the step increase in reactivity and the rapid increase in fission power. The negative reactivity feed-back due to the increase in temperature progressively slows the rate of fission power increase. Eventually, the fission power as well as the temperatures in the different regions of the TFE peak, as the negative reactivity equals the input reactivity [see Fig. 8(a)]. Beyond this point, the total reactivity becomes negative, forcing the fission power and temperatures of the TFE to decrease. Ultimately, steady-state is reached as the net reactivity in the nuclear reactor core becomes equal to zero, ~ 250 seconds after the initiation of the transient.

Figures 9(a) and 9(b) present the results of a negative step input of reactivity of \$0.5. A comparison of the results in Figs. 8(b) and 9(b) indicate that following a positive and a negative reactivity input of \$0.5 the fission power changes initially by as much as +350% and -40%, respectively. This similar, but opposite, response is also indicated not only by the change in the emitter temperature, but also by the changes in the load electric power and conversion efficiency of the TFE [see Figs. 10(a) and 10(b)]. Another major difference in the response of the TFE to

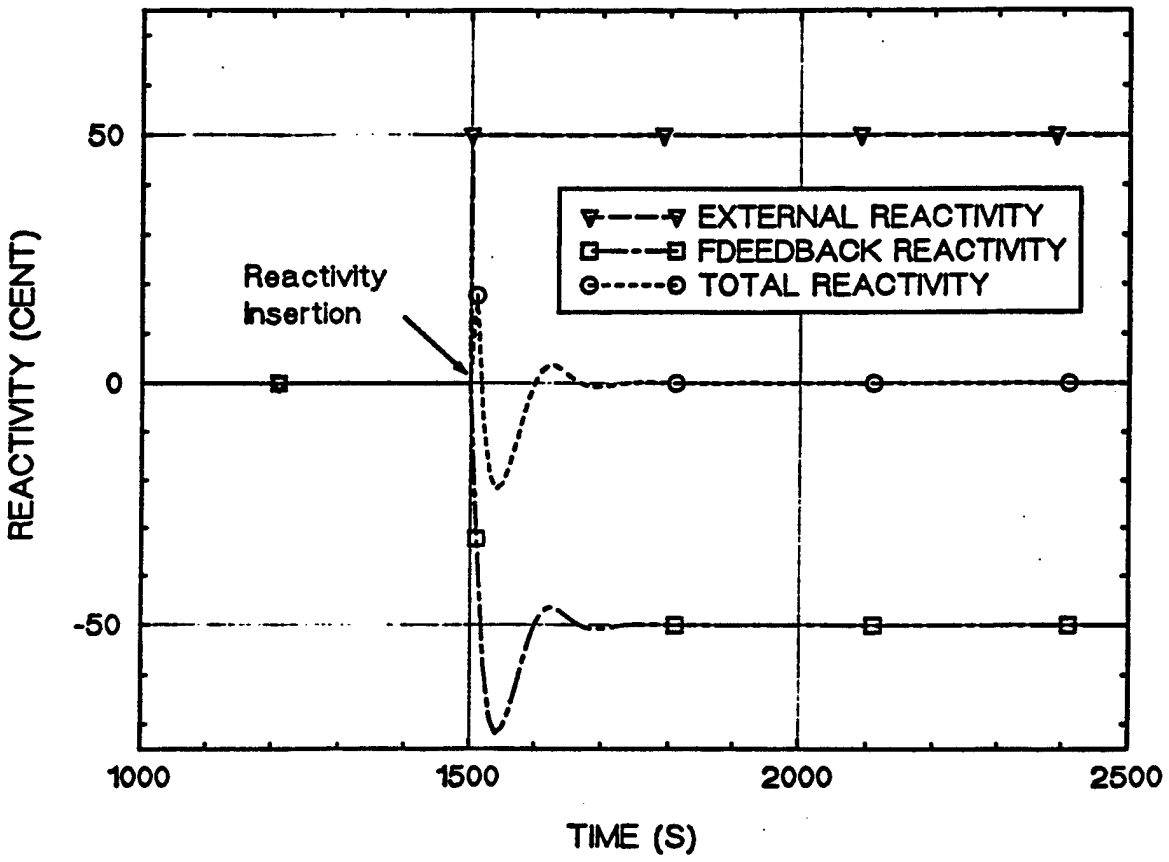

Figure 8(a). Total Reactivity Transient Response to a Positive Step Input in Reactivity of $ 0.5

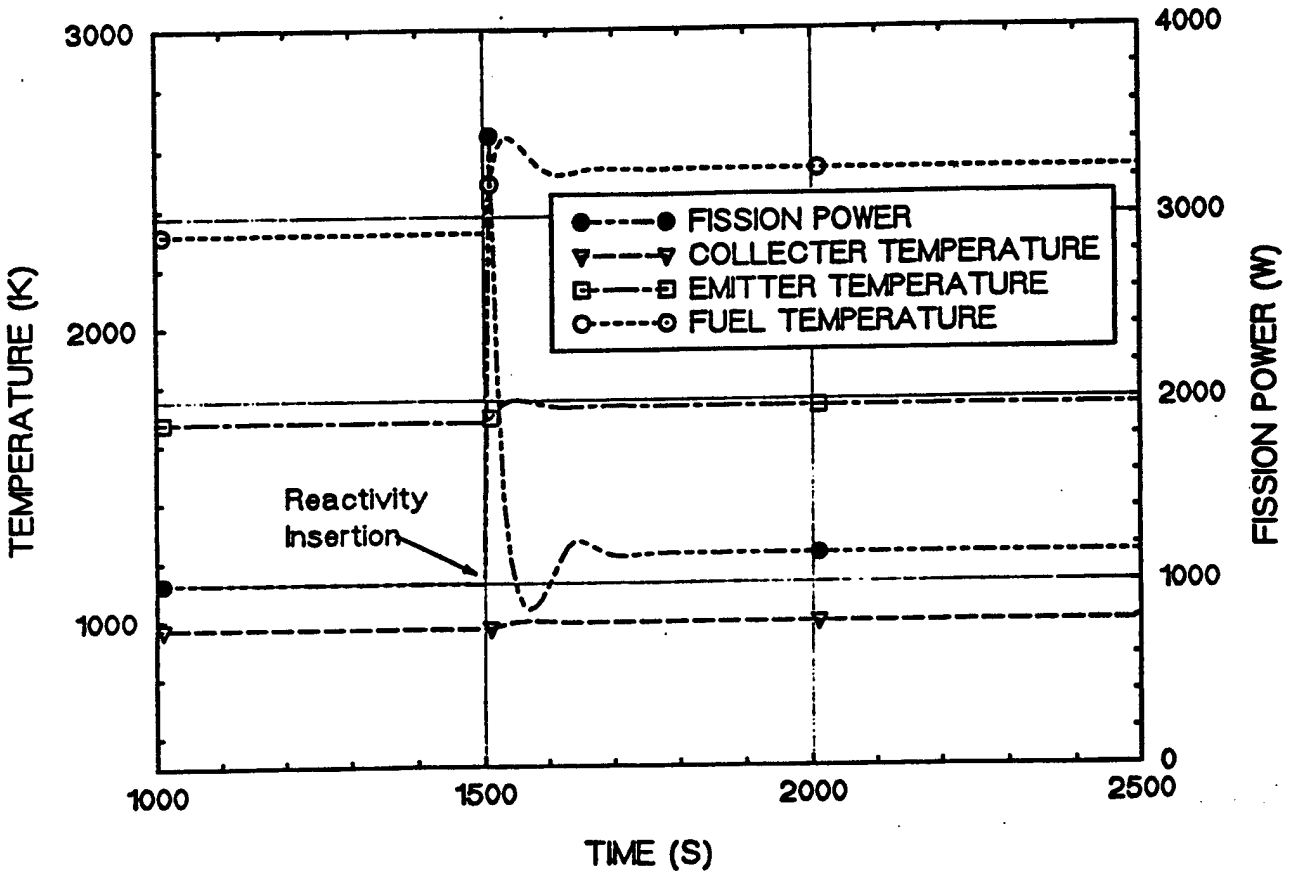

Figure 8 (b). Transient Response of Fission Power and TFE Temperatures to a Positive Step Input in Reactivity of $ 0.5

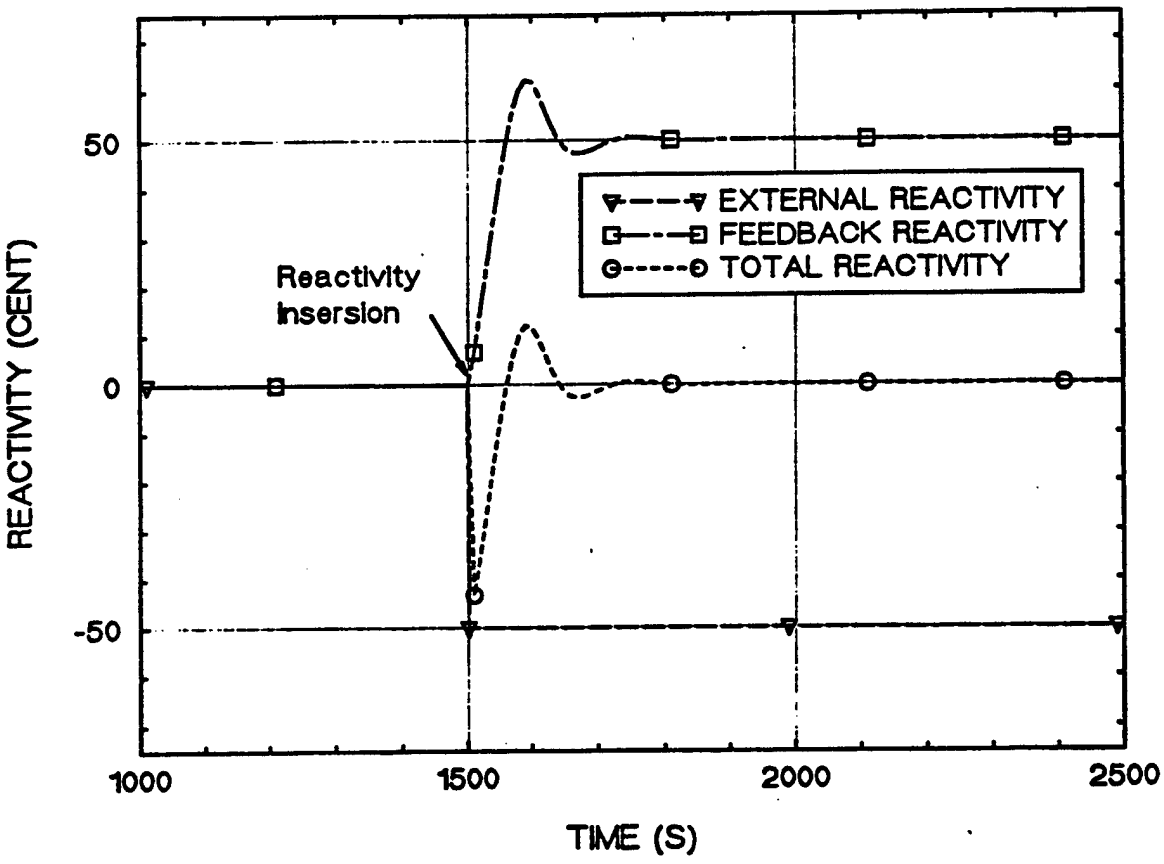

Figure 9 (a). Total Reactivity Transient Response to a Negative Step Input in Reactivity of $ 0.5

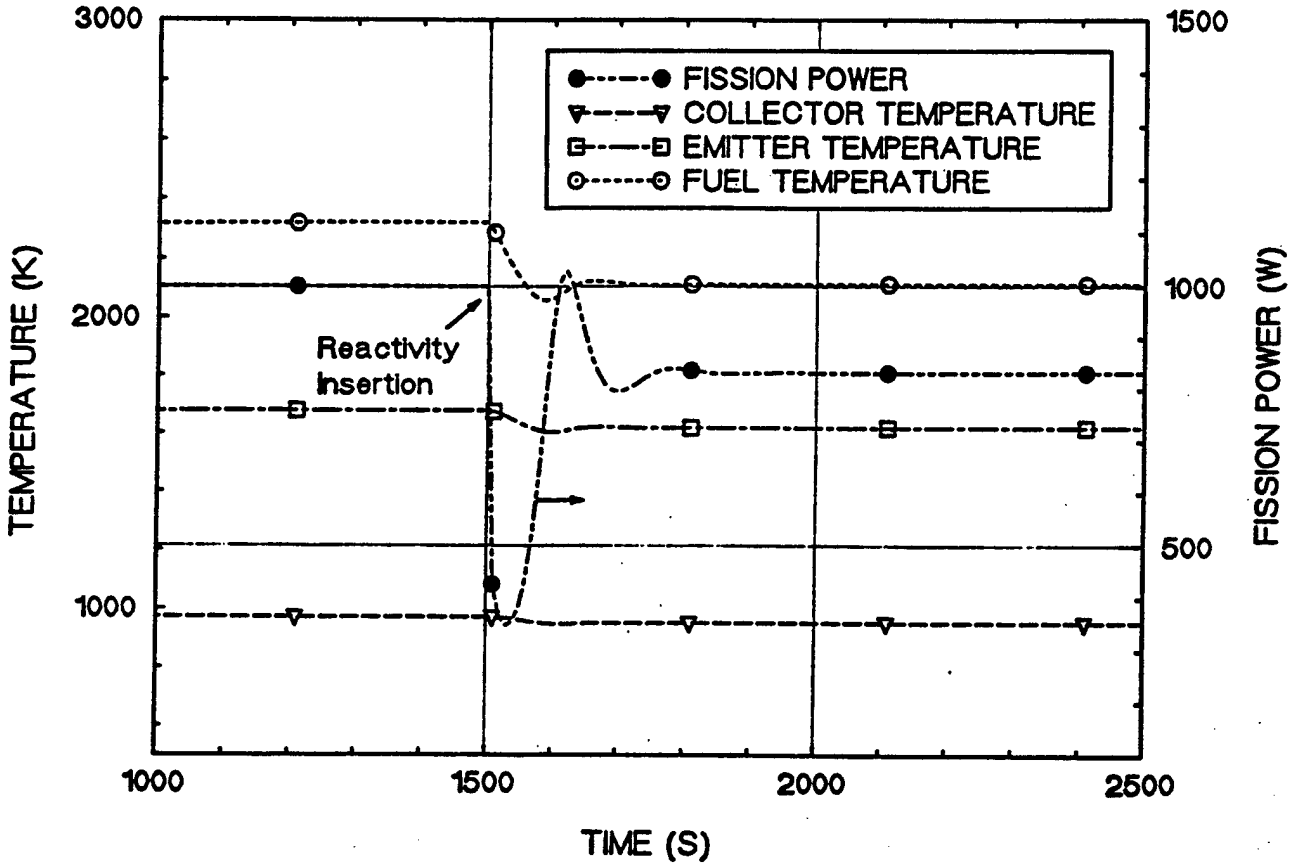

Figure 9(b). Transient Response of Fission Power and TFE Temperatures to a Negative Step Input in Reactivity of $ 0.5

positive and negative reactivity inputs of equal magnitude is that the second peaking in the fission thermal power for the former (1,150 W) is much larger than that for the latter (1,005 W).

In the case of a positive reactivity input of \$0.5, because the initial rise in fission power is accompanied by a much slower rise in load electric power [see Fig. 10(a)], the conversion efficiency of the TEF initially drops precipitously from about 10% to a minimum of 3% [see Fig. 10(b)]. The minimum efficiency corresponds to the peak fission power occurring after the initiation of the transient. Beyond this point, the TFE efficiency begins to rise as the fission power decreases and the load electric power continues to increase, reaching a higher steady-state value of approximately 11 percent; a net increase of one percent. A similar, but opposite responses in the load electric power and TFE conversion efficiency are shown following a negative reactivity input of \$ 0.5 [see Figs. 10(a) and 10(b)].

It is worth noting that the transient response of the TI conversion efficiency is different from that described above for the TFE overall conversion efficiency; the former is based on the thermal power input to the emitter, while the latter is based on the thermal power generated in the fuel region. While the TFE efficiency initially decreases (or increases) following a positive (or negative) step input in reactivity, the TI efficiency increases (or decreases) slowly with time. At steady-state the TI efficiency equals that of the TFE, whereas the fission power becomes equal to the thermal power input to the emitter. At the beginning of the transient, the change in the fission power mainly changes the thermal energy storage in the fuel, and hence its temperature. The thermal input to the emitter changes very slowly with time because of the low thermal diffusivity of the UO_2 fuel and the presence of an open gap between the fuel pellets and the emitter [see Fig. 1].

Figure 11 presents the operating condition before and after the transients on a plot of the J-V characteristics of the TI converter. It can be seen that initially, the TI converter operates in the ignited obstructed mode. As shown in Fig. 11, a positive step input in reactivity of \$0.5 moves the operation conditions of the TI converter closer to the transition point (J', V'), resulting in a higher conversion efficiency and higher load electric power [see Fig. 10(b) and 11]. Conversely, a negative step input in reactivity of \$0.5 moves the operation conditions of the TI converter away

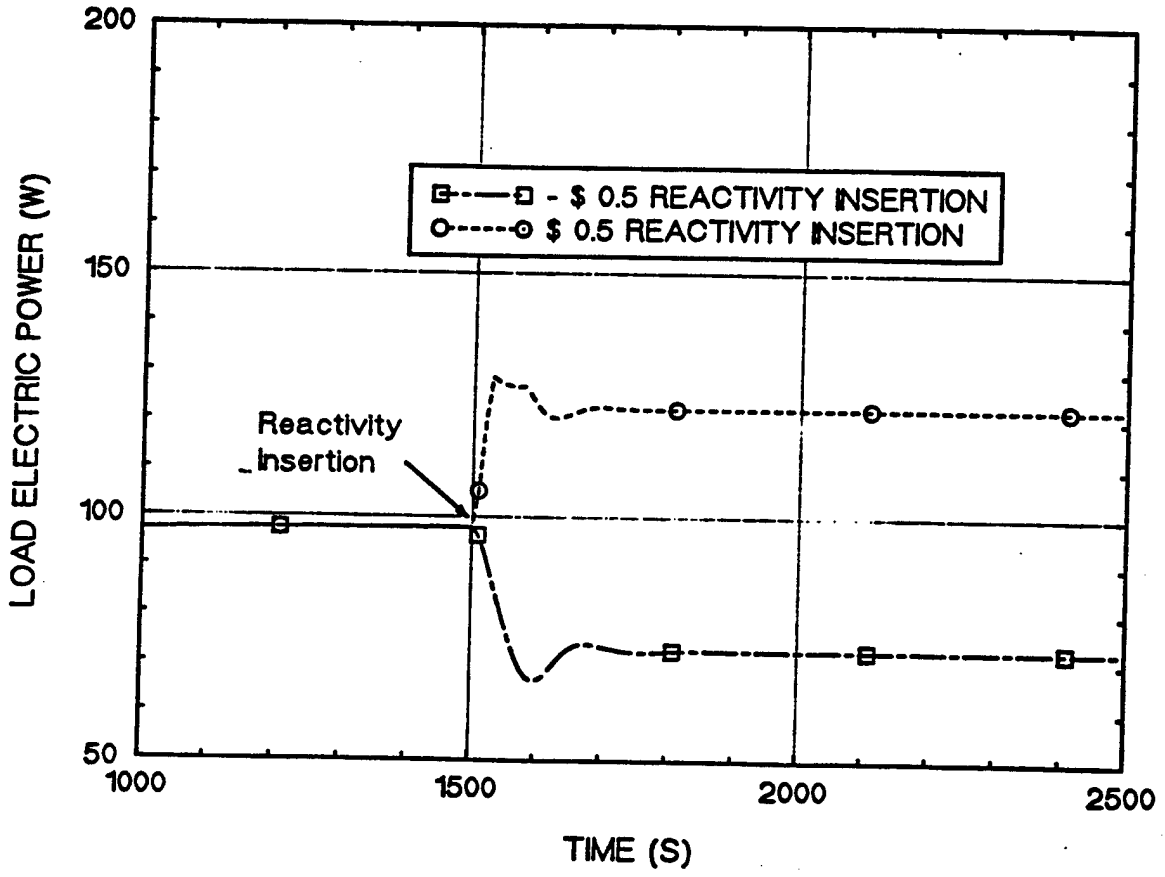

Figure 10(a). Comparison of the Transient Response of Load Electrical Power to a Positive and Negative Step Input in Reactivity of $ 0.5

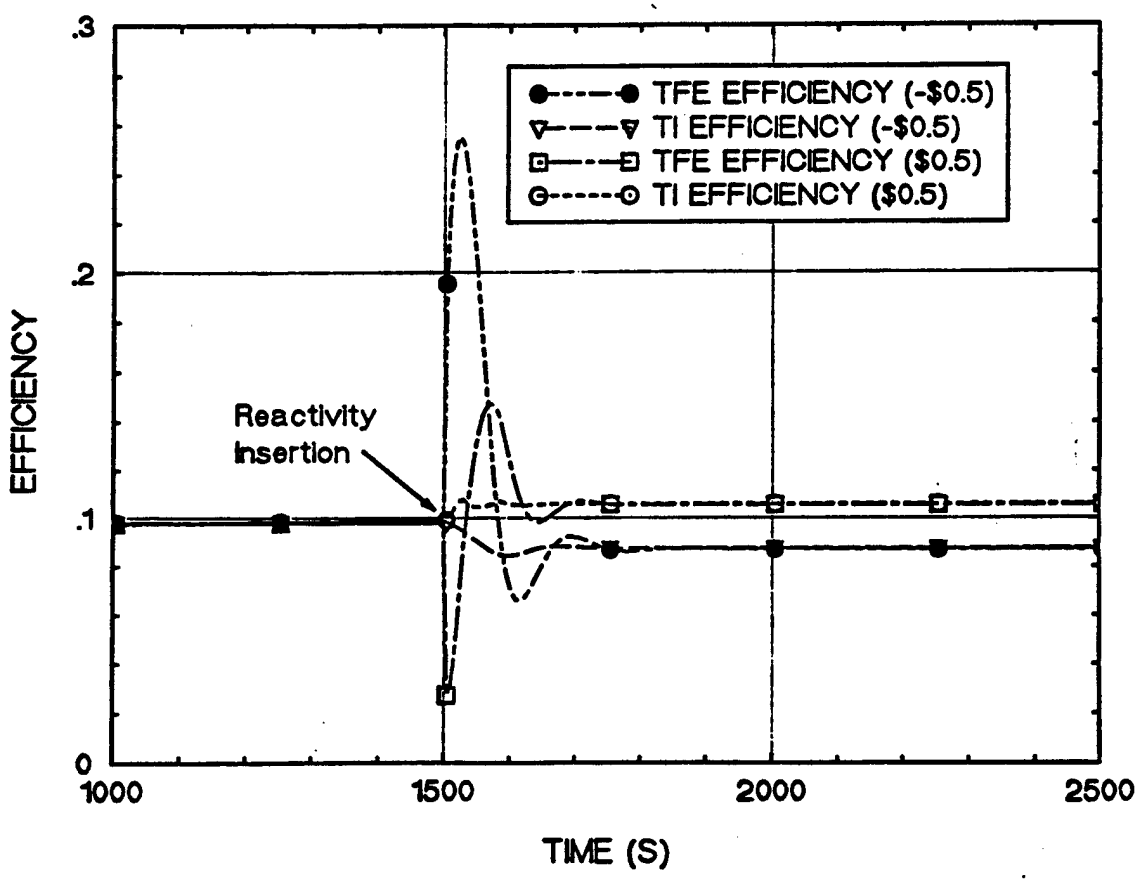

Figure 10(b). Comparison of the Transient Response of TI and TFE Conversion Efficiencies to a Positive and Negative Step Input in Reactivity of $ 0.5

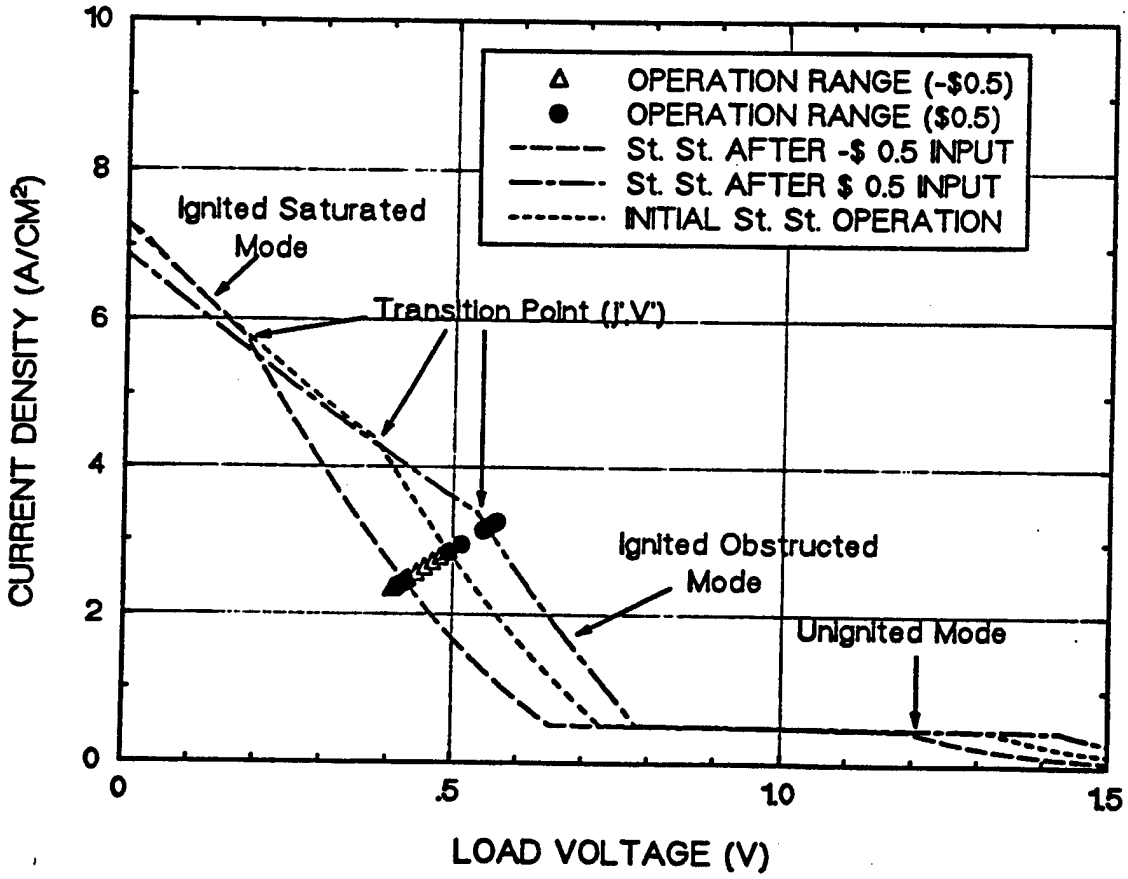

Figure 11. J-V Characteristics Illustrating the Operation Modes of the TFE Following a Positive and Negative Step Input in Reactivity of $ 0.5

from the transition point (J', V'), hence lowering both the TI conversion efficiency and the load electric power.

4.4 Load-Following Characteristics

For an initial steady-state fission power of 1,000 W, Fig. 12 presents the load-following characteristics of the TFE. As this Figure shows, because of the negative temperature reactivity coefficients of the TFE [see Table 1], the nuclear fission power is always load following. An increase in the load electric demand increases electron cooling of the emitter, therefore lowering its temperature and that of the fuel region. Such decrease in temperatures introduces a positive temperature reactivity causing the fission power to increase commensurate with the load demand. Conversely, a decrease in load demand increases the fuel and emitter temperatures, hence lowering fission power due to the negative temperature reactivity feedback effect.

While the fission power is always load-following the integrated TFE is only partially load-following. As demonstrated in Fig. 12, the load electric power for the base case TFE increases with increased load demand; it peaks at 98 W for a 100% load demand. A further increase in load demand is met with a decline in the load electric power. Therefore, the TFE being analyzed (corresponding load resistance is 2.5 mW) is load-following below 100 % load demand and is non load-following at higher load demands. It should be noted that changing the design and operating conditions of the TFE would shift the peak load electric power either to the right or to the left of the point of 100% load demand in Fig.12.

Figure 13 presents an operating surface of the load following characteristics of the TFE. Because of the reactivity feedback effects, changes in load demand causes both the load electrical power and the fission power to change. Figure 13 shows that for a given load electric power there are multiple combinations of fission power and load demand. The contours in Fig. 13 indicate constant load electric power regions. The dark region in Fig. 13 corresponds to the maximum attainable load electric powers between 120 and 140 W for the base design TFE. The results in

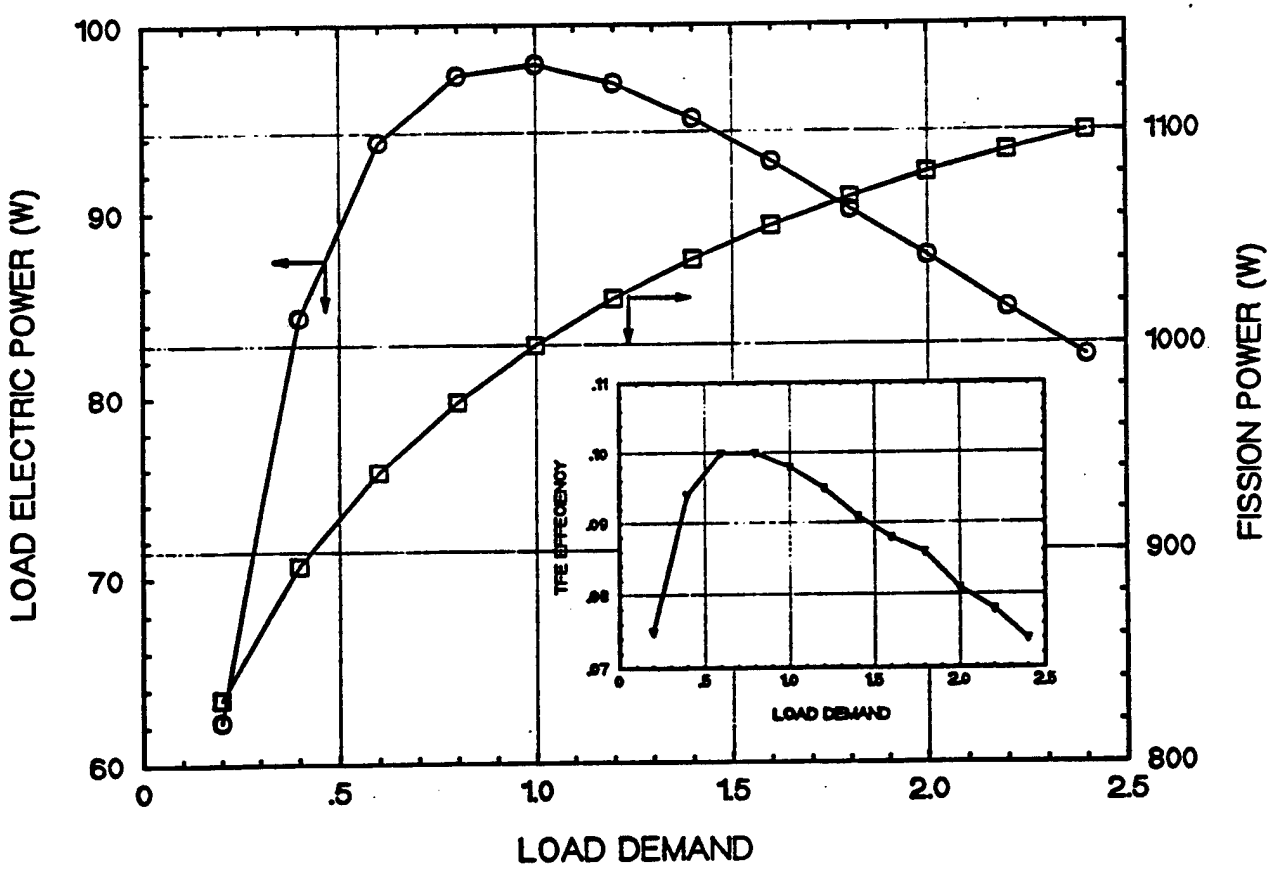

Figure 12. Load-following Characteristics of the TFE Showing the Effect of Changing the Load Demand on Both the Load Electric Power and Fission Power

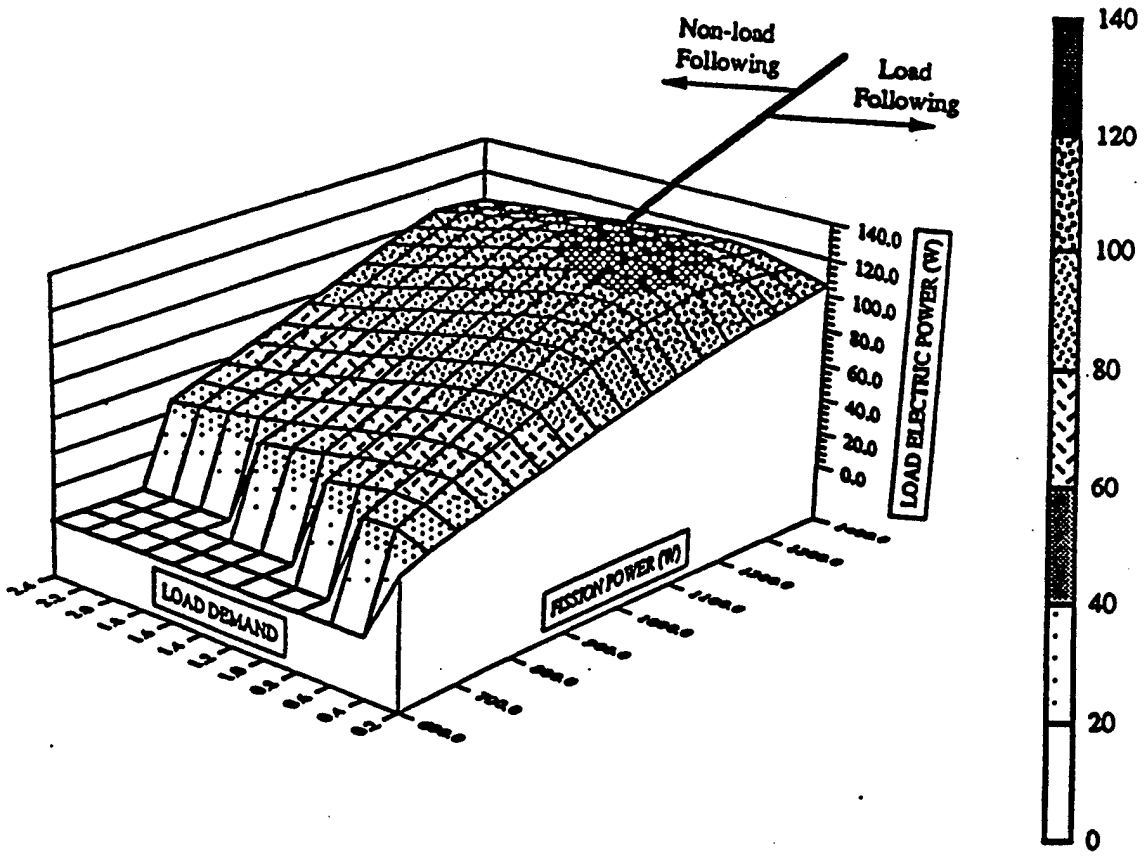

Figure 13. Load-following Operating Surface for the Fully Integrated, Single-cell TFE.

Fig. 13 should be useful to the reactor operator for determining the suitable combinations of load electric power and fission power needed to respond the changes in the load demand.

Results presented in Fig. 14 demonstrate the effect of changing the Cs vapor pressure in the interelectrode gap and/or the width of the gap on the load-following characteristics and the conversion efficiency of the TFE. For the base load demand and for a gap width of 0.25 mm, increasing the Cs vapor pressure from 1.5 torr to 4.0 torr insignificantly affects the load-following response and the conversion efficiency of the TFE, since it does not change the operating condition of the TI converter [see the J-V characteristics in Fig. 11]. However, for a smaller gap of 0.094 mm, increasing the Cs vapor pressure to 4.0 torr shifts the operating conditions of the TI converter closer to the (J', V') transition point, thus increasing both the electric current and the output voltage, resulting in a higher load electric power and a slightly higher efficiency. It should be noted that at high Cs pressure the power losses in the electric leads increases due to the high current density, causing the the load voltage to become very small [see Fig. 15]. Fig. 16(a) shows the effect of changing the Cs vapor pressure and/or the width of the interelectrode gap on the TFE fission power and the emitter temperature, while Fig. 16(b) presents the corresponding effects on the load current and voltage.

These results suggest that in a TI nuclear power system it is desirable at the beginning-of-life to conserve Cs by lowering its vapor pressure, since increasing the Cs pressure would not affect the load electric load of the TFEs. However, should fuel swelling, after operating for an extended period of time, decreases the width of the interelectrode gap, the load electric power will decrease. In this case, the load electric power could be restored by increasing the fission power, and only partially by increasing the Cs vapor pressure in the gap and/or the coolant inlet temperature.

5. SUMMARY AND CONCLUSIONS

A dynamic model that simulates both transient and steady-state operations of fully integrated single-cell TFEs is developed and used to perform parametric analyses. The steady-state analysis investigated the effects of changing the Cs vapor pressure, the width of the interelectrode gap, and

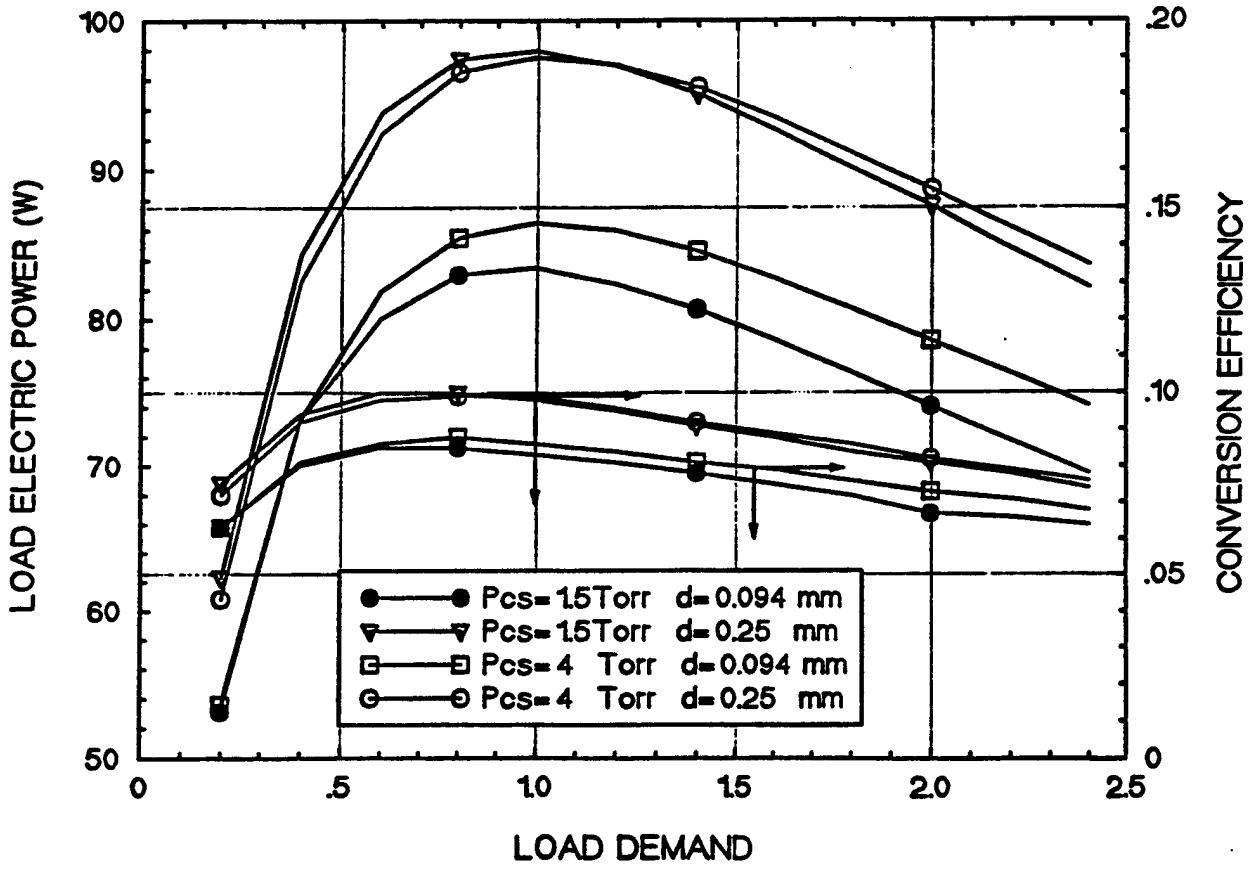

Figure 14. Response of the Load Electric Power and TFE Conversion Efficiency to Changes in the Load Demand

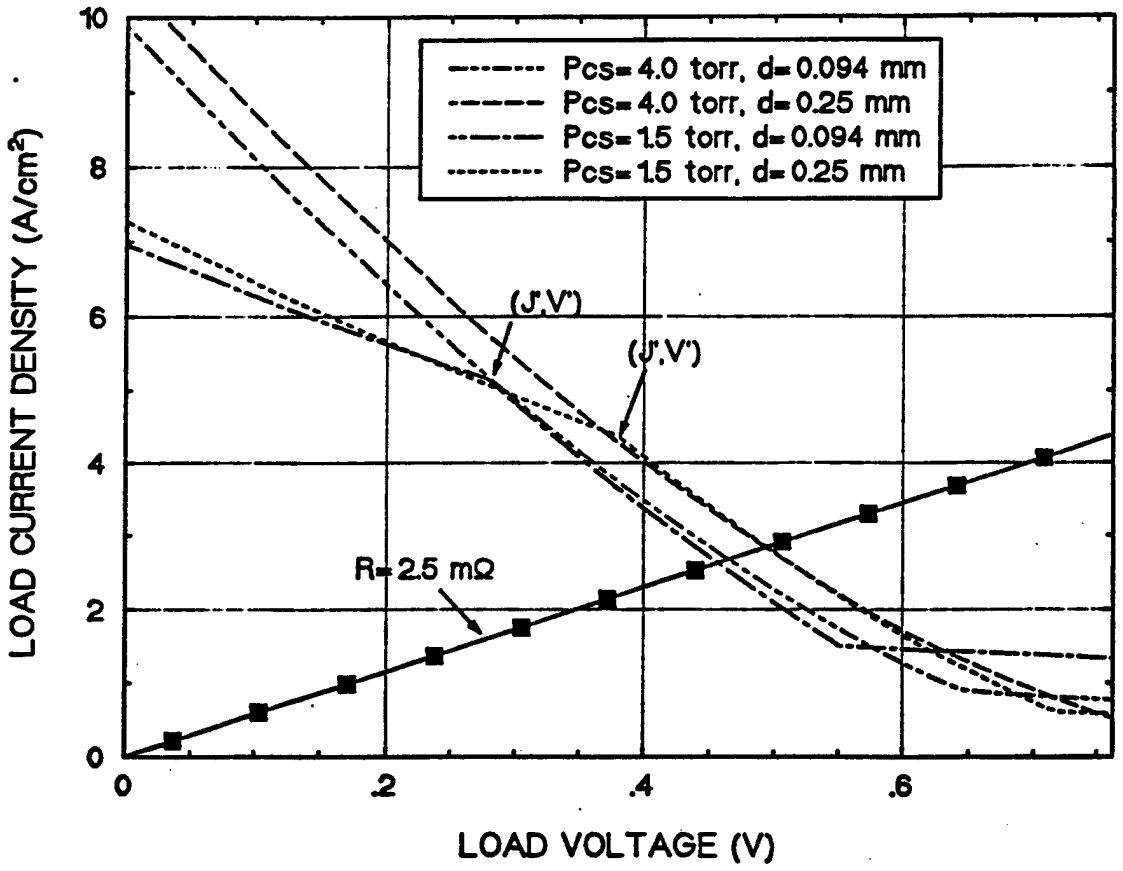

Figure 15. Effect of Cs Pressure and Gap Size on the J-V Characteristics and Operation of the TFE.

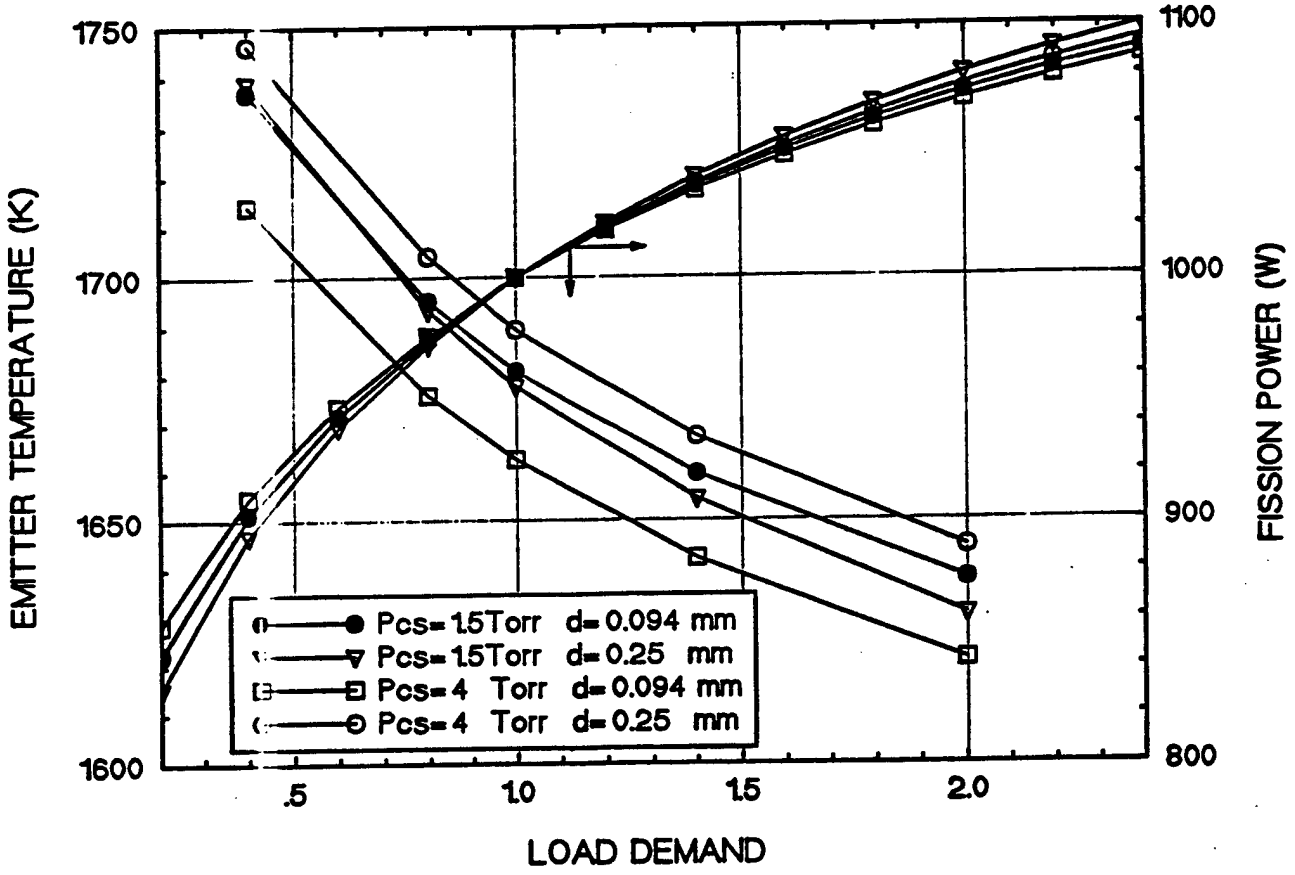

Figure 16(a). Effect of Cs Pressure and Gap Size on the Emitter Temperature and Fission Power as Functions of Load Demand.

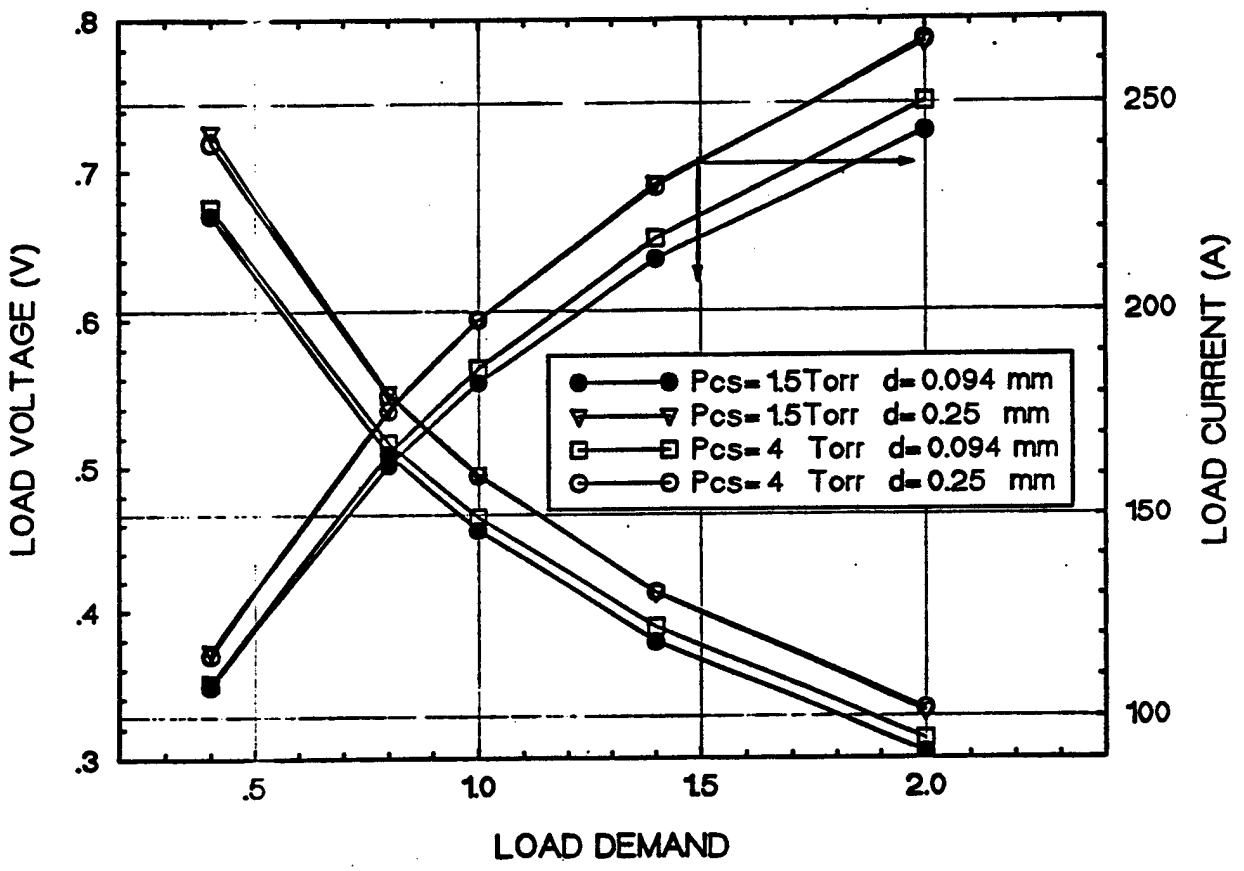

Figure 16(b). Effect of Cs Pressure and Gap Size on the Load Voltage and Current as Functions of Load Demand.

the coolant temperature on the performance as well as the load-following characteristics of the TFE. In addition to these effects, the transient analysis investigated the response of the TFE to a step input in reactivity. The calculated parameters include fission power, load electric power, TFE conversion efficiency, load current and voltage, and temperatures in the different regions of the TFE (fuel, emitter, collector, electric insulator, cladding and coolant) as functions of load demand.

Steady-state results show that the coolant inlet temperature might be used, in addition to the Cs pressure, to regulate the operation of the TFEs. When operating at a high fission power, where the TFE becomes non-load following, it is advisable to lower the inlet coolant temperature in order to improve the TFE performance. Conversely, when operating at low fission power, where the TFE is load-following, increasing the coolant inlet temperature enhances the performance of the TFE. In actual TI power system applications, the inlet coolant temperature to the TFEs could be regulated by controlling the the input power to the electromagnetic pumps which circulate the liquid metal coolant.

Steady-state results also show that increasing the gap size always enhances the performance of the TFE, while increasing the Cs pressure in the interelectrode gap insignificantly affects the TFE performance at low fission powers, but markedly enhance its performance at high fission powers. However, since its desirable to operate the TFE is the load-following regime, it is advisable to lower the Cs pressure, and hence reducing its consumption, with little effect on the TFE operation. On the other hand, the results clearly demonstrate that a reduction in the gap size due to swelling of nuclear fuel would strongly degrade the performance of the TFE.

Transient results show that although a nuclear reactor with negative temperature reactivity coefficients is always load following, the TFEs are only partially load-following. For the TFE base case design and operation parameter, the load electric power peaks at 100% of load demand, which corresponds to a load resistance of 2.5 mW. Beyond this point, increasing the load demand lowers the TFE electric power power output (non load-following regime), while reducing the load demand is accompanied by a reduction in the load electric power (load-following regime). Results also show that for TFEs with large interelectrode gaps, it is desirable at the beginning-of-life to

conserve Cs by lowering its vapor pressure; increasing the Cs pressure would not affect the load electric load. However, should fuel swelling, after operating for an extended period of time, causes the width of the interelectrode gap to decrease, both the TFE conversion efficiency and the load electric power will decrease. In this case, the load electric power might be restored by increasing the fission power, and only partially by increasing the Cs vapor pressure in the interelectrode gap and/or regulating the coolant inlet temperature.

ACKNOWLEDGMENT

Research sponsored by the Strategic Defense Initiative Organization and the Aero Propulsion and Power Directorate, Wright Laboratory, U. S. Air Force, Wright-Patterson AFB under Subcontract No. S-247-002-001 to the University of New Mexico's Institute for Space Nuclear Power Studies.

REFERENCES

[1]NASA, *Report of the 90-Day Study on Human Exploration of the Moon and Mars*, National Aeronautics and Space Administration, City, ST, November 1989.

[2]Bennett, G. L. and A. D. Schnyer, *Proc. of the 8th Symposium on Space Nuclear Power Systems*, CONF-910116, M. S. El-Genk and M. D. Hoover, eds., American Institute of Physics, New York, vol. 1 (6-10 January 1991), pp. 77-83

[3]Harty, R. B., R. E. Durand, and L. S. Mason, *AIAA/NASA/OAI Conference on Advanced SEI Technologies, paper No. AIAA 91-3520*, Cleveland, OH (September 4-6, 1991).

[4]El-Genk, M. S., Morley, N. J., Cataldo, R., and Bloomfield, H., *Proc. 2nd Int. Conf. on the Construction and Operation in Space - Space 90*,Albuquerque, NMAmerican Society of Civil Engineers (23-26 April 1990) .

[5]Morley, N. J. and El-Genk, M. S., *Proc. 8th Symposium on Space Nuclear Power Systems*, Albuquerque, NM, American Institute of Physics, Conference Proceedings No. 217, M.S. El-Genk and M.D. Hoover, eds, vol.1 (6-10 January 1991), pp. 254-252.

[6]Bennett, G., *NASA Nuclear Thermal Propulsion Workshop*, Cleveland, OH, NASA Conference Publication 10079, 10-12 July,1990.

[7]Buden, D, "Operational Characteristics of Nuclear Rockets", *J. Spacecraft*, Vol. 7, No. 7, July, 1970.

[8]El-Genk, M.S., N.J. Morley, and V.E. Haloulakos, *Proc. 8th Symposium on Space Nuclear Power Systems*, CONF-910116, M.S. El-Genk and M.D. Hoover, eds., American Institute of Physics, New York, vol.1 (6-10 January 1991), pp. 607-611a.

[9]Truscello, V. C. and L. L. Rutger, *Proc. of the 9th Symposium of Space Nuclear Power Systems*, Albuquerque, NM, American Institute of Physics, Conference Proceedings No. 217, M.S. El-Genk and M.D. Hoover, eds, vol. 1, (12-15 January 199), pp. 1-24.

[10]Morris, D. B., V. H. Stanley, and M. J. Schuller, *Proc.9th Symposium on Space Nuclear Power Systems*, Albuquerque, NM, American Institute of Physics, Conference Proceedings No. 217, M.S. El-Genk and M.D. Hoover, eds. (12-15 January 1992).

[11]Rasor Associates Inc., *TECMDL-Ignited Mode Planar Thermionic Converter Model*, Report #E563004-C-082988/NSR-31/90-0775, August, 1990.

[12]Pawlowski, R. A., A. Klien, and J. B. McVey, *Proceedings of the 26th IECEC*, vol. 3, (1991) pp. 99-104 .

[13]Peters, R. R and Jekel, T. B, *Proceedings of the 9th Symposium on Space Nuclear Power Systems*, M.S. El-Genk and M.D. Hoover,eds., American Institute of Physics (10-16 January 1992).

[14]Rasor, N. S., *Applied Atomic Collision Physics*, vol. 5, (1982) pp.170-200 .

[15]Houston, J.M., *Advanced Electronics*, vol. 17, (1962) pp.125-206.

[16]Kitrilakis, S. and M. Meeker, Advanced Energy Conversion, vol. 3, (1963) pp. 59-68 .

[17]Burdi, G.F., *SNAP Technology Handbook, Vol. 1: Liquid Metals*, NAA-SR-8617, Reactor Technology, TID-4500 (29th ed.), SNAP Reactors (1964).

[18]Hatsopoulos, G.N. and E.P. Gyftopoulos, *Thermionic Energy Conversion, vol. 1: Processes and Devices*. MIT Press, Cambridge, Massachusetts. (1973).